minerals

MDPI

Article

Elemental Geochemistry and Pb Isotopic Compositions of the Thick No. 7 Coal Seam in the Datun Mining Area, China

Na Meng [1], Qianlong Xiao [2] and Wu Li [2,*]

[1] Jiangsu Key Laboratory of Industrial Pollution Control and Resource Reuse, School of Environmental Engineering, Xuzhou University of Technology, Xuzhou 221018, China; mengna309@163.com
[2] Key Laboratory of Coalbed Methane Resource and Reservoir Formation Process, Ministry of Education, China University of Mining and Technology, Xuzhou 221008, China; ts22010063a31@cumt.edu.cn
* Correspondence: liwu@cumt.edu.cn

Abstract: Thick coal seams recorded abundant petrological, geochemical, and mineralogical information regarding their formation, which in turn can reflect the characteristics of the coal-forming environments, provenance attributes, paleoclimate, and so on. In order to explore the geochemical and lead isotope characteristics of thick coal seams, the No. 7 coal seam in the Datun mining area, Jiangsu Province of China, was selected as the research object. In this work, 29 samples (including coal, roof, and floor rock samples) were collected from three coal mines in the Datun mining area. Through an analysis of the mineral composition and element geochemical characteristics in the coal samples, the enrichment degree of trace elements and modes of rare earth elements were determined. The genetic mechanism of abnormal enrichment of enriched elements is discussed, especially the modes of occurrence and isotope characteristics of Pb. The results showed the following: (1) The main minerals in the coal samples include quartz, potassium feldspar, plagioclase, calcite, dolomite, pyrite, gypsum, and clay minerals, with clay minerals, calcite, quartz, and dolomite being the most common. (2) The major element oxides in coal mainly include SiO_2, Al_2O_3, Fe_2O_3, MgO, CaO, Na_2O, K_2O, TiO_2, P_2O_5, and FeO. In the vertical direction, the variation of SiO_2, Al_2O_3, Fe_2O_3, MgO, K_2O, and FeO in coal samples from the three coal mines is consistent. The average value of Al_2O_3/TiO_2 in the samples of Kongzhuang, Longdong, and Yaoqiao coal mines is 28.09–50.52, which basically locates the samples in the felsic source area, such that the sediment source is considered to be felsic source rock. (3) Elements U, La, Pb, and other elements are more enriched in Kongzhuang coal mine samples; elements Th, U, La, Pb, and other elements are more enriched in the Longdong coal mine samples; and elements Th, U, La, Pb, and other elements are more enriched in the Yaoqiao coal mine samples. Furthermore, W is enriched in Yaoqiao mine samples and is highly enriched in Longdong mine samples. The mining area is generally rich in the elements U, La, and Pb. The distribution curves of rare earth elements in the three mines are inclined to the right, with negative Eu anomalies. The enrichment is of the light rare earth enrichment type. (4) Pb isotope data show that the samples from the three mines are mainly distributed in the orogenic belt and the subduction zone lead source areas, where the upper crust and the mantle are mixed, with individual sample points distributed in the mantle and upper crust lead source areas.

Keywords: Pb isotope; trace elements; thick coal seam; Datun mining area

check for updates

Citation: Meng, N.; Xiao, Q.; Li, W. Elemental Geochemistry and Pb Isotopic Compositions of the Thick No. 7 Coal Seam in the Datun Mining Area, China. *Minerals* **2024**, *14*, 848. https://doi.org/10.3390/min14080848

Academic Editor: Shifeng Dai

Received: 1 July 2024
Revised: 18 August 2024
Accepted: 18 August 2024
Published: 22 August 2024

Copyright: © 2024 by the authors. Licensee MDPI, Basel, Switzerland. This article is an open access article distributed under the terms and conditions of the Creative Commons Attribution (CC BY) license (https://creativecommons.org/licenses/by/4.0/).

1. Introduction

The formation process of coal is affected by a variety of geological and geochemical factors [1–3]. Coal can retain geological information, especially thick seams, which record more complete information [4–6]. Coal seams can be divided into extremely thin (0.3–0.5 m), thin (0.5–1.3 m), medium-thick (1.3–3.5 m), thick (3.5–8 m), and extremely thick (>8 m) coal seams [7].

Coal is a special kind of sedimentary organic rock composed of organic and inorganic components [8,9]. Under certain geological and geochemical conditions, it can enrich a variety of elements [1,10–12]. Research on the content and characteristics of elements in coal not only enables reconstruction of the coal-forming environment and clarifies basic theoretical problems, such as the regional geological history evolution of coal-bearing strata, but also has important significance for the development of critical elements in coal and coal-bearing sequences and therefore can enhance the clean utilization of coal [13–19]. With the development of technological advances, more and more studies on elemental geochemistry have attracted attention, and the concentration, distribution, and modes of occurrence of elements in coal have been further investigated [20–25]. For example, through electron microprobe analysis (EPMA), it was found that rare earth elements and yttrium (REY)-containing phosphate existed in the clay minerals, and the discovery of monazite as a dispersed mineral in the magnesium–aluminum silicate matrix may be derived from debris and monazite-containing chlorite, indicating that monazite is formed through hydrothermal alteration during coalification [26]. Mineralogical studies using X-ray diffraction have shown that quartz and kaolinite are the main mineral phases of coal in the West Bokaro coalfield, India, and the results indicated that Cu and Cr are closely related to minerals, while Co mainly exists in organic form [27]. The three coal seams in the Ningdong Coalfield, Ordos Basin, China are enriched in Mn, Sr, and Ba, where the enrichment degrees of Sr and Ba varied between coal 18 (Sr is 85 μg/g, Ba is 80 μg/g), coal 6 (Sr is 230 μg/g, Ba is 421 μg/g) and coal 4-2 (Sr is 1667.06 μg/g, Ba is 741.69 μg/g) [24]. Therefore, there are differences in the vertical occurrence of elements in coal seams, especially with respect to the enrichment degree of trace elements [1,28–30]. In a stable sedimentary environment, even with magmatic-hydrothermal solutions, some critical elements will be only formed and enriched in local areas, which has been confirmed by several researchers [31–40].

Lead is one of the main harmful elements in coal [41,42]. Although the content of lead in coal is typically relatively low [12], it will be released during the combustion, processing, and utilization of coal, causing harm to the environment and human health [43]. Previous studies have found that lead in coal mainly occurs as an inorganic mineral, in the form of galena (PbS), and some lead exists in sulfate, carbonate, phosphate, and silicate, especially in coal with a poor sulfide content [44–46]. Swaine [47] and Finkelman et al. [41] showed that lead may occur in pyrite, and its organic association in low-rank coal is also possible. In the early stages of research, it was found that the content of lead in the coal seam of the Datun mining area was abnormal [48]. Therefore, it is necessary to analyze the elemental content and occurrence mode of lead, given its high level in coal, and to reveal its source by means of lead isotope analysis.

In recent years, more and more researchers have studied the lead isotope in thick coal seams and coal [19,49–53]. However, there have been few reports on the vertical stratigraphic changes of geochemical characteristics in thick coal seams. Due to differences in composition and their high thickness, the geochemical characteristics of thick coal seams may present some differences in the vertical direction [36,37]. In this study, a total of 29 samples were collected from the No. 7 coal seam system of three mines in the Datun mining area, Jiangsu Province, China. Through analyses including XRD, XRF, ICP-MS, lead isotope analysis, and other methods, the mineralogy, geochemistry, and lead isotope characteristics of the No. 7 coal seam are investigated, and it is hoped that this can provide a theoretical basis for the clean utilization of this coal.

The concentrations of major and trace elements in the study area were analyzed and studied. The modes of occurrence characteristics of minerals and elements were also assessed, and the lead isotopes in the samples were tested. Additionally, the possible sources and evolution pathways of the lead present in coal in this area were obtained. The results of this study have certain significance regarding the material sources and influencing factors of Pb and other metal elements in coal in this area. At the same time, it promotes the

exploration and development of measures for critical metals in coal, potentially addressing scientific problems related to regional geological evolution.

2. Samples and Methods

2.1. Samples Collected

The coal mines presented in this study were located in the Datun mining area in Xuzhou City, Jiangsu Province, China (Figure 1). Following the Chinese standard GB/T 482-2008, the samples were cut into 10 cm wide and 10 cm deep sections and stored in plastic bags to prevent contamination and oxidation. The No. 7 coal seam at Kongzhuang, Yaoqiao, and Longdong coal mines in the Datun mining area was sampled using a stratified channel. Datun mining area is located in Fengpei synclinorium, forming an east–west zoned, north-rising, and south-falling, north-oblique fault block coal field. The three coal mines are all hidden coalfields. The coal seams are Carboniferous–Permian coal seams. The collected samples were from the early Permian Shanxi Formation, and the coal rank was bituminous coal. The three coal mines are about five kilometers apart from each other.

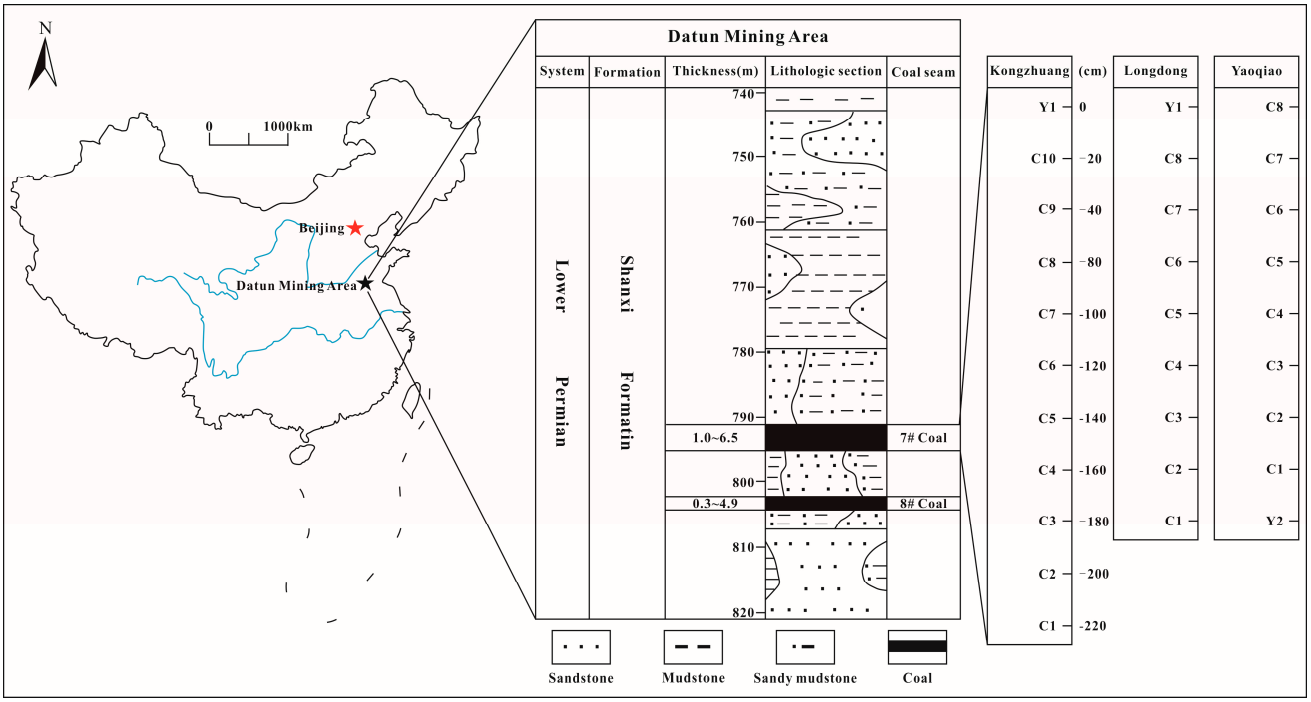


Figure 1. Location of the study area and stratigraphic column, with sample per mine indicated.

Samples were taken from the bottom of the No. 7 coal seam at intervals of 20 cm. The samples were fresh samples of coal seam, roof, and floor rocks exposed in the mine. Coal and rock samples were directly carved from the mining face or roadway, and coal samples were collected from coal seams using steel sampling boxes of corresponding sizes. A total of 29 coal, roof, and floor samples were collected, including 26 coal samples, 2 roof rock samples, and 1 floor rock sample (Figure 1, Table 1). Among them, sample KZ-Y1 and sample LD-Y1 denote the top rock samples, sample YQ-Y2 is the bottom plate rock sample and the others are the coal seam samples. Additionally, an appropriate number of samples were collected for elemental analysis and testing.

Table 1. Results of proximate analysis and total sulfur analysis of coal samples (%).

Mine	Sample	M_{ad}	A_d	V_{daf}	FC_d	St_d
Kongzhuang	KZ-C1	1.65	9.79	37.55	56.34	0.81
	KZ-C2	2.72	24.24	42.50	43.56	1.67
	KZ-C3	2.63	32.76	44.74	37.16	1.93
	KZ-C4	1.80	6.80	39.29	56.58	0.57
	KZ-C5	1.58	7.86	38.11	57.02	0.59
	KZ-C6	1.68	7.28	36.92	58.48	0.49
	KZ-C7	1.57	9.00	38.19	56.24	0.45
	KZ-C8	1.44	9.59	38.87	55.27	0.49
	KZ-C9	1.60	13.74	36.07	55.14	0.41
	KZ-C10	1.81	6.74	35.97	59.71	0.51
	KZ-Y1	1.74	88.83	99.18	0.09	1.71
Longdong	LD-C1	3.48	9.16	40.23	54.30	1.33
	LD-C2	2.44	8.77	36.8	57.66	0.67
	LD-C3	2.66	11.14	38.15	54.96	0.62
	LD-C4	2.32	16.69	30.47	57.92	0.72
	LD-C5	2.26	12.18	38.80	53.74	0.61
	LD-C6	2.56	8.88	37.28	57.15	0.62
	LD-C7	2.50	14.23	31.39	58.85	0.62
	LD-C8	2.78	12.15	39.95	52.76	0.71
	LD-Y1	0.22	92.79	95.27	0.34	0.50
Yaoqiao	YQ-C1	1.90	7.03	40.00	55.78	0.55
	YQ-C2	2.02	6.53	34.85	60.89	0.53
	YQ-C3	1.91	6.30	34.98	60.92	0.51
	YQ-C4	2.17	7.20	38.18	57.38	0.55
	YQ-C5	1.80	6.52	39.49	56.57	0.53
	YQ-C6	2.04	9.94	35.80	57.82	0.43
	YQ-C7	1.92	9.54	35.48	58.36	0.58
	YQ-C8	2.08	7.88	39.27	55.94	0.71
	YQ-Y2	1.33	83.55	70.55	4.84	0.41

Notes: M, moisture; A, ash yield; V, volatile matter; FC, fixed carbon; St, total sulfur; d, dry basis; daf, dry and ash-free basis; ad, air-dry basis.

2.2. Experimental Methods

According to the Chinese standards GB/T 212-2008 (proximate analysis of coal. This standard is applicable to lignite, bituminous coal, anthracite coal, and coal water slurry) and GB/T 214-2007 (determination of total sulfur in coal), coal samples are burned in an oxygen stream under the action of a catalyst, and sulfur in the coal is converted into sulfur oxides. These oxides are absorbed by a hydrogen peroxide solution to form sulfuric acid, which is then titrated with a sodium hydroxide solution. The total sulfur content in the coal is calculated based on the amount of standard sodium hydroxide solution consumed; the proximate analysis and total sulfur analysis of coal samples were carried out at the Jiangsu Institute of Geology and Mineral Resources Design (Testing Center of China Coal Geology Administration). Mineral composition analysis and Pb isotope tests were completed at the China Institute of Nuclear Industry Geology.

FeO was finished by methods for chemical analysis of silicate rocks. Part 14: Determination of ferrous oxide content (GBT14506.14-2010), while major elements were tested by methods for chemical analysis of silicate rocks. Part 28: Determination of 16 major and minor elements content (GBT14506.28-2010). The major elements in the sample were tested using a ME-XRF26 X fluorescence spectrometer: 1 g of 200 mesh powder sample was dried in an oven at 100 °C, then burned in a high-temperature furnace higher than 1000 °C for 2 h to determine its loss on ignition (LOI). The burned sample was weighed to 0.5 g, which was mixed with 4 g of $Li_2B_4O_7$ solvent in a plastic bottle, and 0.4 g 1% LiBr and 0.5% NH_4I flux were added to the platinum crucible for XRF. The mixed sample was melted at 1250 °C to form a glass cake and determined through XRF.

The mass fraction of trace elements and rare earth elements in the sample was determined using inductively coupled plasma mass spectrometry (ICP-MS): 1 g of 200 mesh rock powder sample was put into the melting tank, 2 mL of 8 mol HNO_3, and 0.5 mL of 8 mol HF were added, and the sample was heated on an electric heating plate (at about 100 °C) until the sample was completely dissolved. The melting tank was opened, and the sample was evaporated in the fume cupboard. The sample was heated and evaporated again by adding 2 mL 8 mol HNO_3. Finally, the sample solution dissolved in 8 mol HNO_3 was diluted with deionized water to 250 mL and put into a clean solution bottle. After shaking, 10 mL was taken and put into a small plastic tube for testing. The contents of various elements were determined through ICP-MS using the ME-ICP61 four-acid digestion method, and the contents of rare earth elements were determined through ICP-MS using the ME-MS81 method.

The lead isotope analysis test was completed at the Beijing Research Institute of Uranium Geology (BRIUG), China, and the Pb isotope ratio was determined through four-acid digestion plasma mass spectrometry. The sample was decomposed via four-acid digestion (HNO_3-$HClO_4$-HF-HCl), and the detection instrument was ICP-MS. First, 0.5 g of the sample was weighed and digested by a mixed solution of $HClO_4$, HF, HNO_3, and HCl. After drying, the sample was heated using an electric heating plate and leached with HCl. The cooled solution was diluted to 25 mL with 10% HCl and analyzed using high-precision ICP-MS. During the detection process, a Pb isotope reference material and internal standard were used to control the precision and accuracy.

3. Results and Discussion

3.1. Mineralogy

Minerals are important components of coal [54–57]. Their types and modes of occurrence not only reflect information regarding the environment and provenance during the formation of coal seams but also affect the distribution and modes of occurrence of trace elements in coal [55,58].

The mineral results of the samples from the three mines included quartz, potassium feldspar, plagioclase, calcite, dolomite, pyrite, gypsum, and clay minerals, of which the major minerals were clay minerals, calcite, quartz, and dolomite. In the samples from the Kongzhuang mine (Figure 2), most of the samples were dominated by clay minerals and calcite. The clay mineral content of sample KZ-C2 was the highest of these samples, while the clay mineral content of sample KZ-C7 was the lowest. Sample KZ-C2 and sample KZ-C3 did not contain calcite and only small amounts of pyrite and gypsum. Sample KZ-Y1 rock samples only contained quartz and clay minerals. The contents of quartz and calcite in sample KZ-C7 were higher than those in other coal samples. The samples from the Longdong mine (Figure 3) were dominated by clay minerals and calcite, with small amounts of gypsum, dolomite, pyrite, and plagioclase. Sample LD-C4 had the highest content of clay minerals (up to 98.6%). The mineral content of the roof rock sample (LD-Y1) was mainly quartz (64.3%), along with certain proportions of potassium feldspar, plagioclase, and clay minerals. In the samples from Yaozhuang mine (Figure 4), the clay minerals accounted for the highest proportion, with the highest content of 97% (sample YQ-C2), sandwiched with calcite, dolomite, quartz, pyrite, and potassium feldspar. Sample YQ-Y2 quartz content in the floor rock sample was 34.7%, the potassium feldspar content was 1.9%, and the clay mineral content was 63.4%. The content of pyrite in the coal samples from the Yaoqiao mine is higher than those from the other two coal mines.

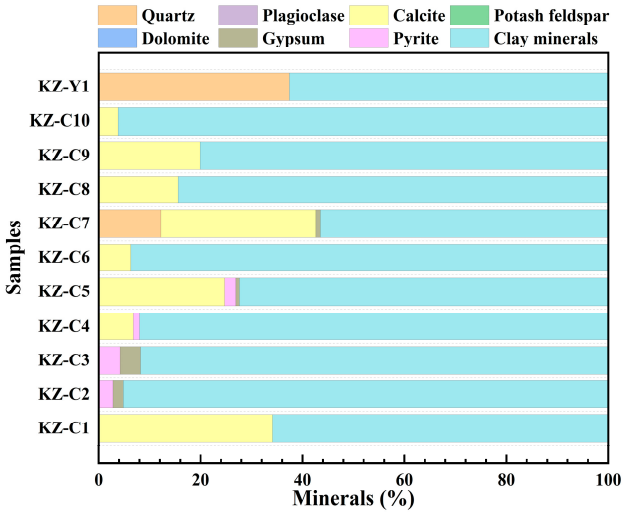


Figure 2. Mineral content composition diagram of Kongzhuang mine samples.

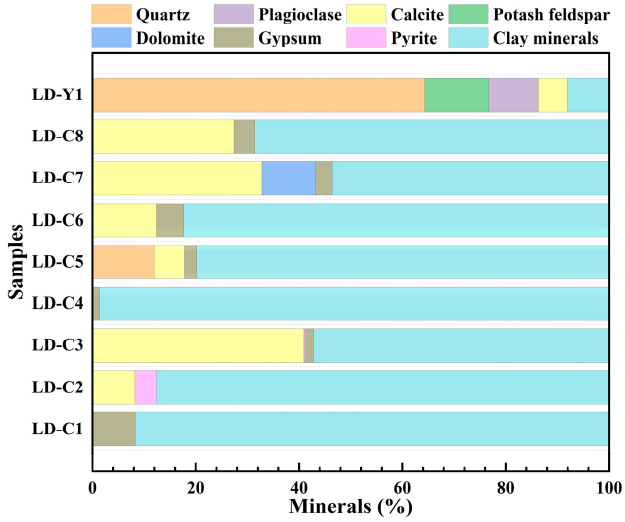


Figure 3. Mineral content composition diagram of Longdong mine samples.

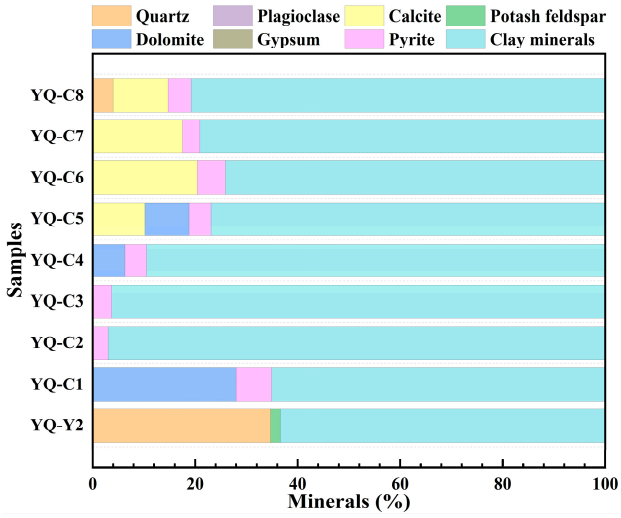


Figure 4. Mineral content composition diagram of Yaoqiao mine samples.

3.2. Geochemical Features

3.2.1. Major Element Oxides

The inorganic chemical components of coal mainly include SiO_2, Al_2O_3, Fe_2O_3, MgO, CaO, Na_2O, K_2O, MnO, TiO_2, P_2O_5, and FeO. The contents of major element oxides in coal in the study area are shown in Table 2, where the contents of SiO_2 and Al_2O_3 were found to be the highest. SiO_2 mainly exists in the form of clay minerals and quartz, while Al_2O_3 mainly exists in clay minerals and hydroxides (e.g., boehmite) in coal, as reported by some researchers [13,34,37,59]. Sulfide minerals, carbonate minerals, and sulfate minerals might contain Fe_2O_3, which represents the forms of iron ore (e.g., hematite, siderite) in coal. Like SiO_2 and Al_2O_3, TiO_2 in coal mainly derives from the supply of sediment-source region during mudstone deposition. TiO_2 is a lithophile element that mainly appears in the form of rutile and anatase in coal. Fe_2O_3, CaO, MgO, Na_2O, and K_2O are alkaline oxides. When there are more alkaline oxides in coal, the ash melting point will decrease [60].

Table 2. The contents of major element oxides in samples (%).

Mine	Sample	SiO_2	Al_2O_3	Fe_2O_3	MgO	CaO	Na_2O	K_2O	TiO_2	P_2O_5	Loss on Ignition	FeO
Kongzhuang	KZ-C1	3.31	3.36	0.63	0.12	1.26	0.15	0.03	0.12	0.04	90.56	0.41
	KZ-C2	13.93	11.63	1.72	0.18	0.75	0.13	0.19	0.26	0.02	71.13	0.73
	KZ-C3	16.51	13.53	2.39	0.17	0.72	0.12	0.25	0.26	0.03	65.95	0.93
	KZ-C4	2.72	2.45	0.39	0.08	0.69	0.10	0.02	0.03	0.01	93.36	0.31
	KZ-C5	3.00	2.72	0.35	0.08	0.61	0.09	0.01	0.03	0.01	92.82	0.29
	KZ-C6	5.11	4.05	0.43	0.11	0.64	0.10	0.02	0.27	0.02	89.17	0.25
	KZ-C7	4.91	3.06	0.54	0.10	3.76	0.08	0.03	0.28	0.01	87.16	0.20
	KZ-C8	2.41	2.02	0.31	0.09	0.91	0.08	0.02	0.04	0.01	94.02	0.26
	KZ-C9	6.26	5.18	0.38	0.07	1.53	0.08	0.04	0.18	0.01	86.12	0.29
	KZ-C10	6.65	5.46	0.24	0.08	0.58	0.06	0.03	0.09	0.01	86.42	0.20
	KZ-Y1	58.49	22.36	3.92	0.70	0.26	0.27	2.3	0.62	0.06	10.82	2.34
Longdong	LD-C1	2.47	2.05	0.75	0.06	0.60	0.07	0.04	0.05	0.01	93.85	0.54
	LD-C2	5.50	4.65	0.84	0.09	0.90	0.05	0.05	0.30	0.01	87.53	0.44
	LD-C3	2.47	2.09	0.60	0.15	3.43	0.04	0.03	0.11	0.01	90.93	0.35
	LD-C4	5.96	5.06	0.55	0.11	0.39	0.04	0.06	0.17	0.01	87.56	0.29
	LD-C5	8.48	6.61	0.80	0.11	0.94	0.06	0.09	0.31	0.02	82.31	0.49
	LD-C6	3.32	2.77	0.54	0.12	1.19	0.08	0.05	0.08	0.01	91.11	0.35
	LD-C7	3.35	2.71	0.43	0.14	2.90	0.05	0.03	0.10	0.01	89.77	0.31
	LD-C8	4.42	3.66	0.80	0.13	3.99	0.13	0.05	0.08	0.01	86.64	0.44
	LD-Y1	74.75	11.39	0.85	0.29	3.00	1.35	2.73	0.40	0.04	5.08	0.41
Yaoqiao	YQ-C1	4.32	3.79	1.16	0.18	0.40	0.04	0.02	0.05	0.01	89.98	0.25
	YQ-C2	3.26	2.90	0.35	0.06	0.14	0.08	0.02	0.05	0.01	93.01	0.25
	YQ-C3	5.11	4.53	0.36	0.06	0.11	0.10	0.02	0.06	0.01	89.58	0.30
	YQ-C4	3.99	3.88	0.44	0.15	0.46	0.22	0.02	0.04	0.01	90.01	0.25
	YQ-C5	2.75	2.48	0.65	0.18	1.32	0.09	0.02	0.04	0.02	92.32	0.31
	YQ-C6	4.18	3.6	0.39	0.06	0.25	0.13	0.02	0.08	0.02	91.25	0.32
	YQ-C7	5.32	4.65	0.51	0.10	1.52	0.07	0.02	0.16	0.02	87.54	0.34
	YQ-C8	9.14	7.64	0.80	0.11	0.50	0.10	0.07	0.82	0.02	80.67	0.34
	YQ-Y2	56.64	23.28	1.14	0.54	0.40	0.14	1.92	0.78	0.04	15.04	0.87
Average in coal	KZ	6.48	5.35	0.74	0.11	1.15	0.10	0.06	0.16	0.05	/	0.39
	LD	4.50	3.70	0.66	0.11	1.79	0.07	0.05	0.15	0.01	/	0.40
	YQ	4.76	4.18	0.58	0.11	0.59	0.10	0.03	0.16	0.02	/	0.30

From Figure 5, it can be seen that except for P_2O_5 and CaO, other oxides in roof rock samples from the Kongzhuang mine were higher than those from coal seams. In the vertical direction, the concentrations of SiO_2, Al_2O_3, Fe_2O_3, MgO, K_2O, and FeO in major-element

oxides gradually decreased from the maximum value in sample KZ-Y1 to KZ-C4, then increased to sample KZ-C3. The content of CaO increased first and then decreased from top to bottom, reaching a maximum at sample KZ-C7. The content of Ti decreased first and then increased from top to bottom, then increased and decreased. The content of P_2O_5 was very low only at sample KZ-C1, and the upper samples presented values lower than the detection limit. As shown in Figure 6, most of the inorganic elements in the roof rock samples of Longdong Mine were higher than those in the coal seam samples. Therefore, the major element oxides basically decreased from top to bottom, with the contents in individual samples from the coal seam being more prominent. The contents of CaO, MnO, and TiO_2 in coal fluctuated. The variation of inorganic constant element contents in the Yaoqiao mine was similar to that in the other two mines. The contents of K_2O and P_2O_5 were very low; the content of CaO in the roof rock sample was lower than that in the coal sample; the content of Na_2O in sample YQ-C4 was the highest; and the content of TiO_2 in YQ-C8 was the highest (Figure 7).

Comparing the content changes of major-element oxides in the vertical direction for the three mines, it can be seen that the trends of different major-element oxides were relatively consistent, while the contents of Na_2O and TiO_2 in Yaoqiao Mine were quite different from those in other mines. The contents of major-element oxides in the Kongzhuang mine were higher than those in the Longdong and Yaoqiao mines, but the content of Na_2O was higher in the Yaoqiao mine. In addition, the contents of P_2O_5 and FeO were very low in Longdong Mine and Yaoqiao Mine, while the content of P in sample KZ-C1 of Kongzhuang Mine was the highest, and the content of FeO was the highest in samples KZ-Y1 and KZ-C2.

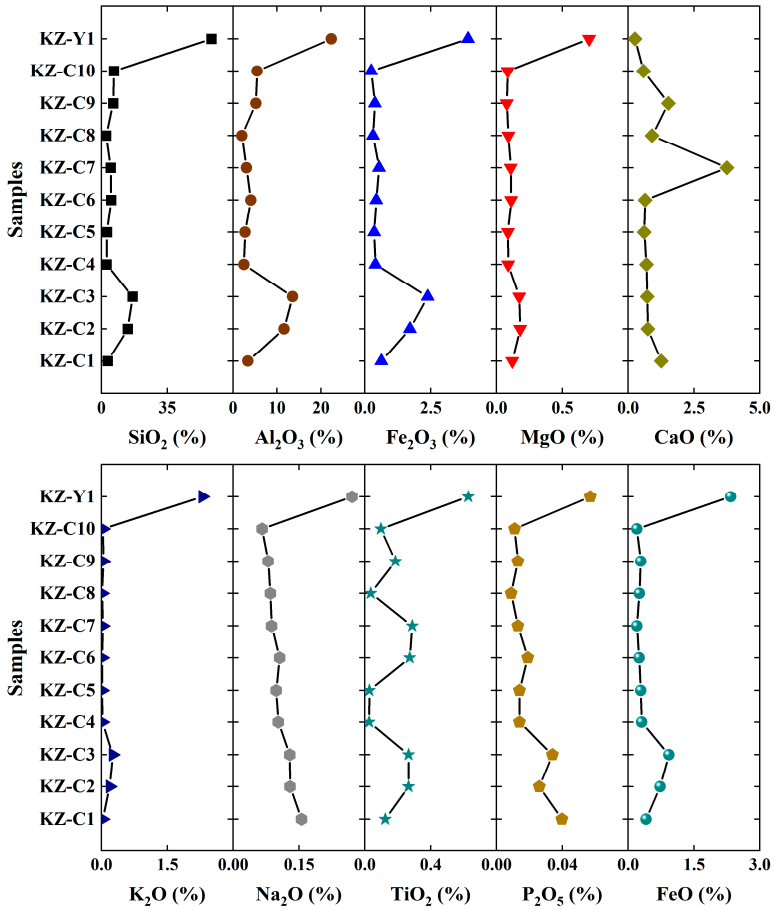


Figure 5. Variation of major-element oxides (%) in the Kongzhuang mine samples.

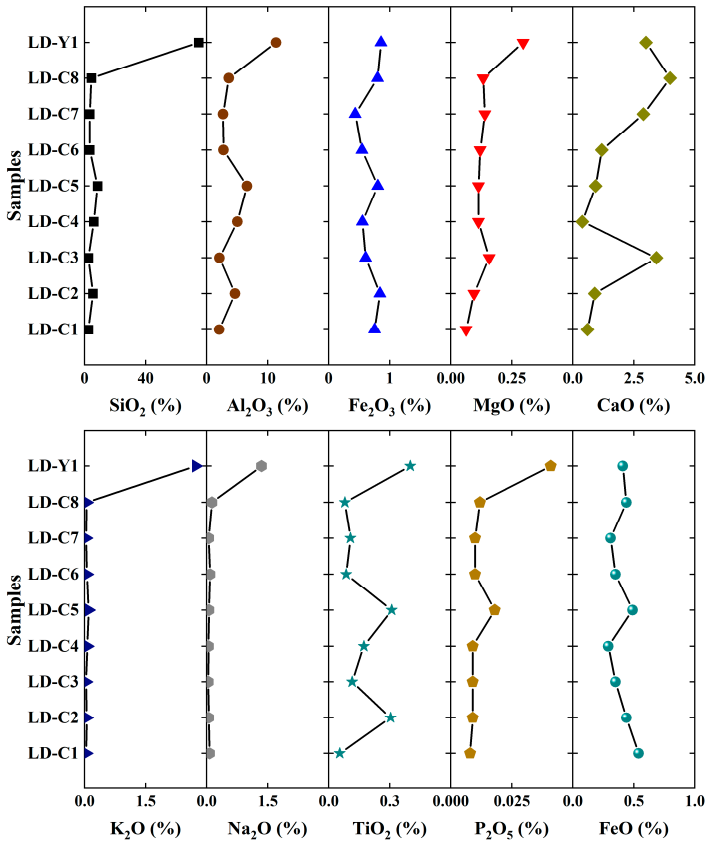


Figure 6. Vertical variation of major-element oxides (%) in the Longdong mine samples.

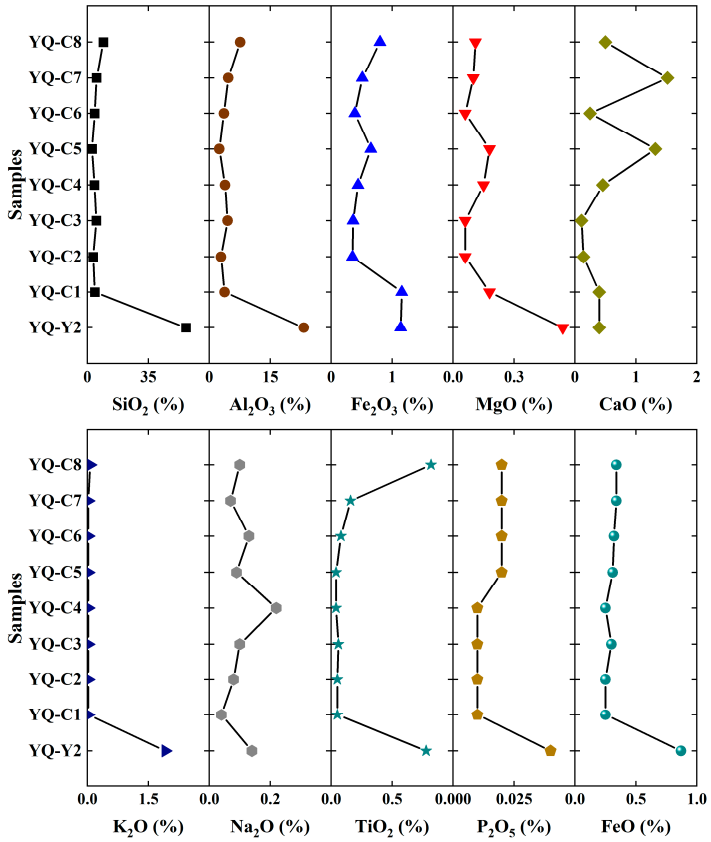


Figure 7. Vertical variation of major-element oxides in Yaoqiao mine samples.

After the formation of the coal seam, the surrounding rock of the roof and floor will exchange material through direct contact with the coal sample and, so, the contents of major-element oxides (e.g., SiO_2, Al_2O3, Fe_2O_3, and other elements) in the coal adjacent to the surrounding rock will be higher than those in the coal far away from the surrounding rock [39]. The elements far away from these latter coal samples, such as Na_2O in YQ-C4 of Yaoqiao mine and CaO in samples from the three mines, may be more related to the material input of the sedimentary environment during the formation of the coal seam and less affected by the surrounding rock.

Using the mean values of the constant elements in the coal samples from the three mines (Table 2), the horizontal distribution of the elements in the coal seam of the study area can be obtained, as shown in Figure 8. The distributions can be mainly divided into five types, as follows: SiO_2, Al_2O_3, and P_2O_5 are the largest in Kongzhuang Mine, followed by Yaoqiao Mine, and the smallest in Longdong Mine; Na_2O and TiO_2 are the largest in Yaoqiao Mine, followed by Kongzhuang Mine, and the smallest in Longdong Mine; the distribution of Fe_2O_3 and K_2O in Kongzhuang Mine, Longdong Mine, and Yaoqiao Mine presents an inverted V-type shape, which decreases in turn; the inverted V-shaped distribution of MgO is the largest in Longdong Mine, followed by Yaoqiao Mine, and the smallest in Kongzhuang Mine; finally, CaO and FeO contents are the highest in Longdong Mine, followed by Kongzhuang Mine, and the lowest in Yaoqiao Mine.

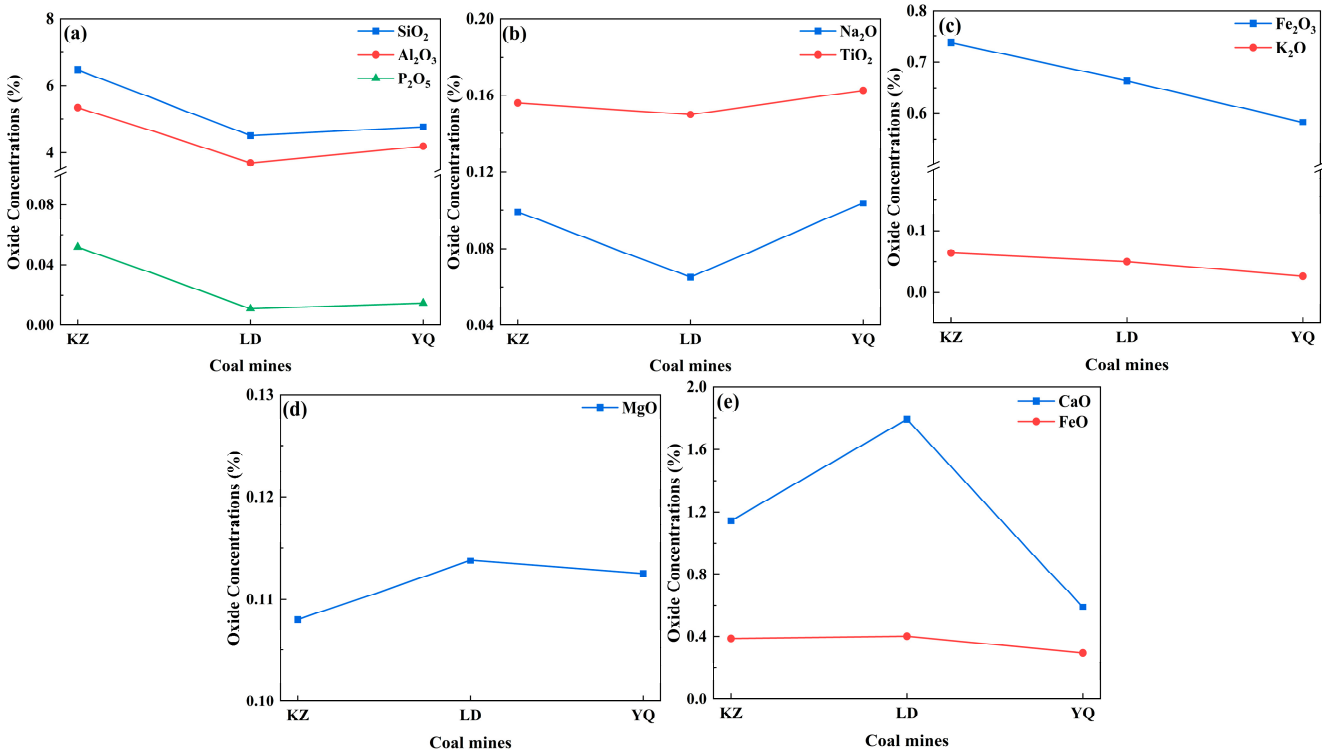


Figure 8. The distributions of major-element oxides in the three coal mines. (**a**) SiO_2, Al_2O_3, and P_2O_5; (**b**) Na_2O, TiO_2; (**c**) Fe_2O_3, K_2O; (**d**) MgO; (**e**) CaO and FeO.

The average content of SiO_2 in coal samples from the No. 7 coal seam in the Datun mining area was 5.34%, accounting for the main position in the major-element oxides, followed by Al_2O_3 with 4.48%. According to the correlation analysis, the correlation between Si and ash is positive (R^2 = 0.65), while the correlation coefficient between Al_2O_3 and ash was similar (R^2 = 0.64). It can be seen, from the mineral results, that the minerals in coal were mainly clay minerals, with a small amount of quartz.

Fe mainly exists in the form of pyrite in coal. The average content of Fe_2O_3 in the coal samples from the No. 7 coal seam in the Datun mining area was 0.67%, and Fe was significantly correlated with the total sulfur content (R^2 = 0.76). Therefore, pyrite was

the main carrier of Fe_2O_3 and is also the main occurrence state of S in coal. Due to the existence of gypsum in coal, as determined in the XRD analysis, S may also occur in gypsum. According to the mineral results, calcite accounted for a large proportion of minerals in the coal samples, second only to clay minerals. Therefore, it can be inferred that CaO mainly exists in the coal samples in the form of calcite.

The chemical properties of Al_2O_3 and TiO_2 are relatively stable during the deposition process. Therefore, the ratio of Al_2O_3/TiO_2 is commonly used as an effective index for judging the source type of coal and coal measures in sedimentary rocks. Hayashi et al. [61] proposed the classification basis of Al_2O_3/TiO_2, in which magnesia-iron is associated with a value of 3–8, intermediate with a value of 8–21, and felsic source rock with a value of 21–70. This ratio has also been widely used for coal and coal-bearing sequences [37,62–65]. The provenance judgment for the study area is shown in Figure 9. It can be seen that the samples of Kongzhuang, Longdong, and Yaoqiao mines were basically categorized into the felsic source area and, so, it is considered that the sediment source in the study area is felsic source rock.

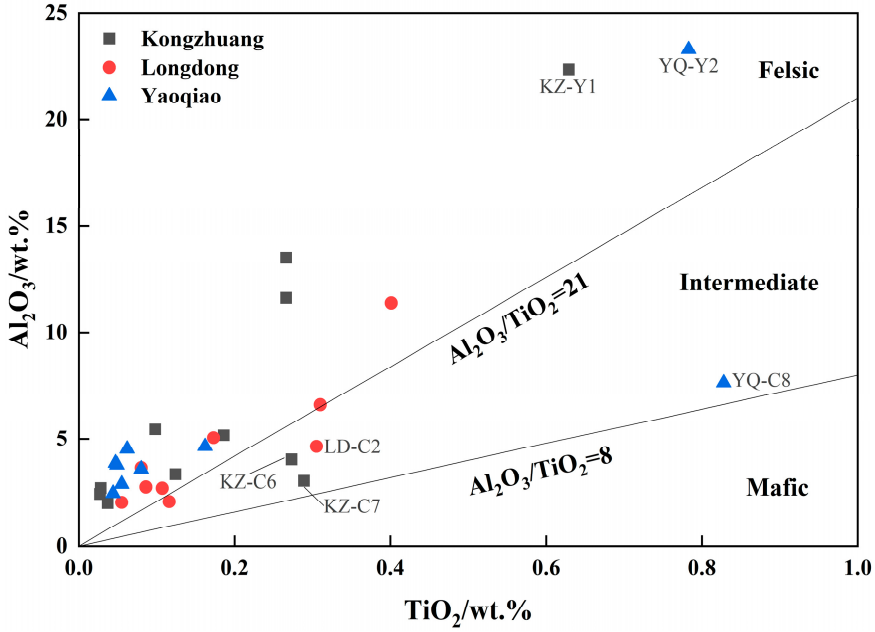


Figure 9. Source identification of Al_2O_3/TiO_2 ratio in the study area [61].

3.2.2. Trace Elements

Based on the concentration coefficients (CC) proposed by Dai et al. [66]—that is, the ratio of the mass fraction of trace elements in coal to the background value of the element in coal in the world or China—the enrichment degrees of trace elements in coal were judged. The enrichment degree can be divided into six grades: depleted (CC < 0.5), normal (0.5 < CC < 2), slightly enriched (2 < CC < 5), enriched (5 < CC < 10), significantly enriched (10 < CC < 100), or unusually enriched (CC > 100). The mean values of world hard coals were obtained from Ketris and Yudovich [67], and the mean values of common Chinese coals were obtained from Dai et al. [33].

The concentration coefficients of most trace elements in the samples from the Kongzhuang mine were between 0.5 and 2. Compared with the world coal, the Kongzhuang mine samples were relatively depleted in Cd, Sb, and Bi and slightly enriched in Li, V, La, and W. Compared with Chinese coal, elements including Be, Cd, Sb, Ho, Tm, Bi, Nb, Ta, and Hf were found to be depleted (Figure 10). Compared with the world coal, Longdong Mine samples were relatively depleted in Be, Cd, Cs, and Bi; slightly enriched in Ce; and significantly enriched in W. The occurrence of W may be related to carbonate minerals and may also belong to sulfophile minerals. Compared with Chinese coal, most trace elements are depleted, including Be, Y, Cd, Sb, Cs, Pr, Nd, Sm, Eu, Gd, Tb, Dy, Er, Ho, Tm, Yb, Lu, Bi,

Nb, Ta, Zr, and Hf, was observed (Figure 11). Compared with the world coal, Yaoqiao coal samples were relatively depleted in Cd, Cs, Tm, and Bi; slightly enriched in Li and Sr; and enriched in W. Compared with Chinese coals, elements including Be, Y, Mo, Cd, Sb, Gd, Dy, Ho, Yb, Lu, Bi, and Hf were found to be depleted (Figure 12).

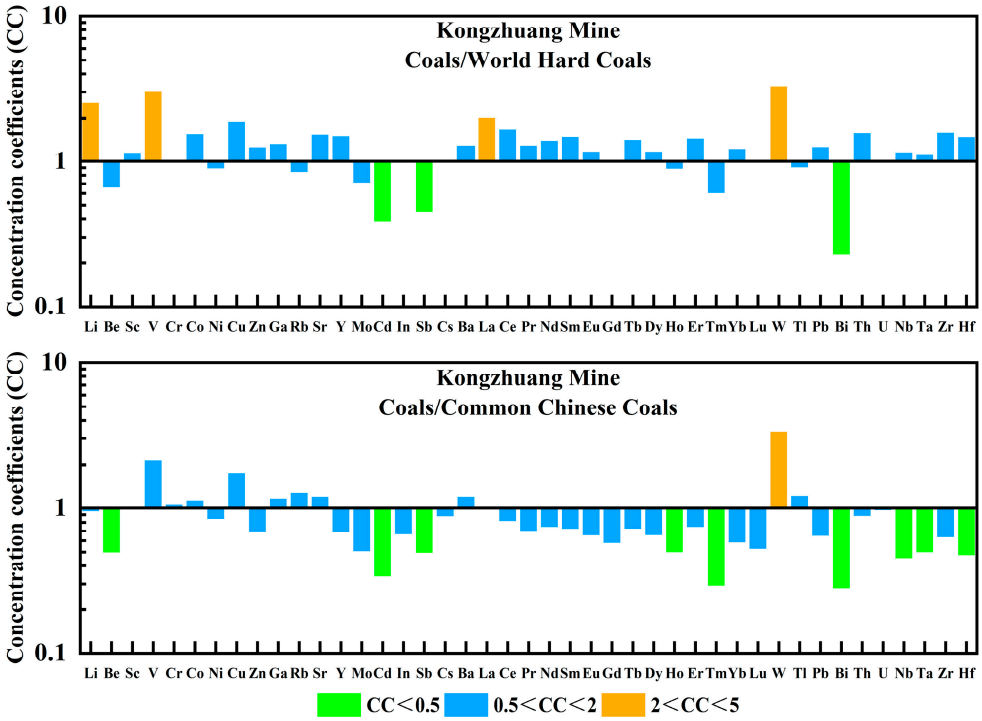


Figure 10. Concentration coefficients (CC) of trace elements in Kongzhuang mine samples (normalized to world coals and Chinese coals).

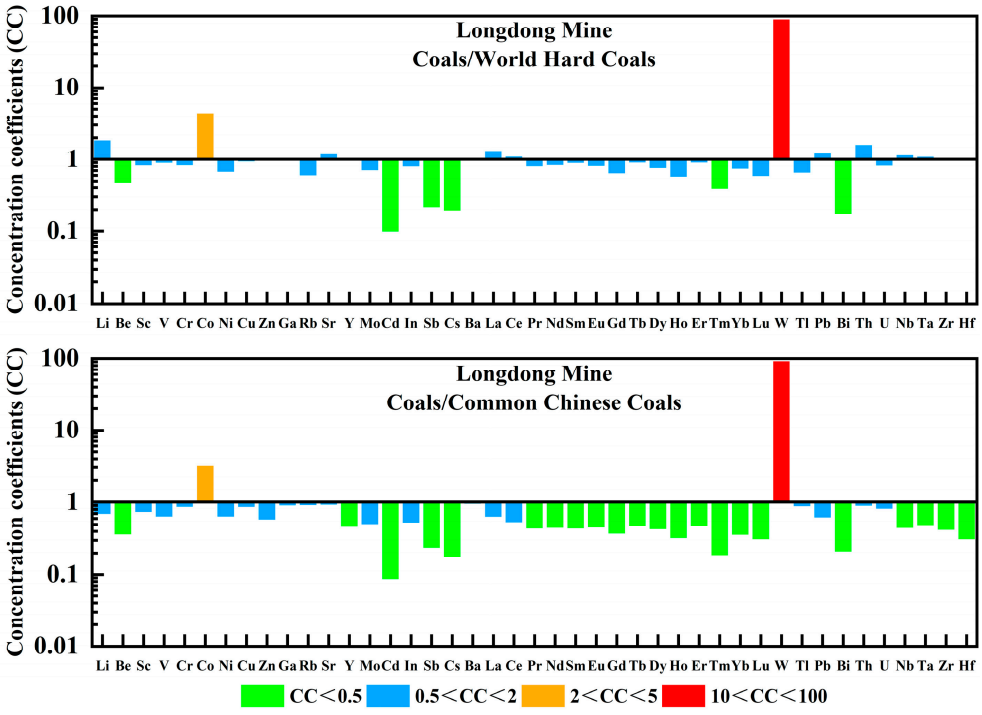


Figure 11. Concentration coefficients (CC) of trace elements in Longdong mine samples (normalized to world coals and Chinese coals).

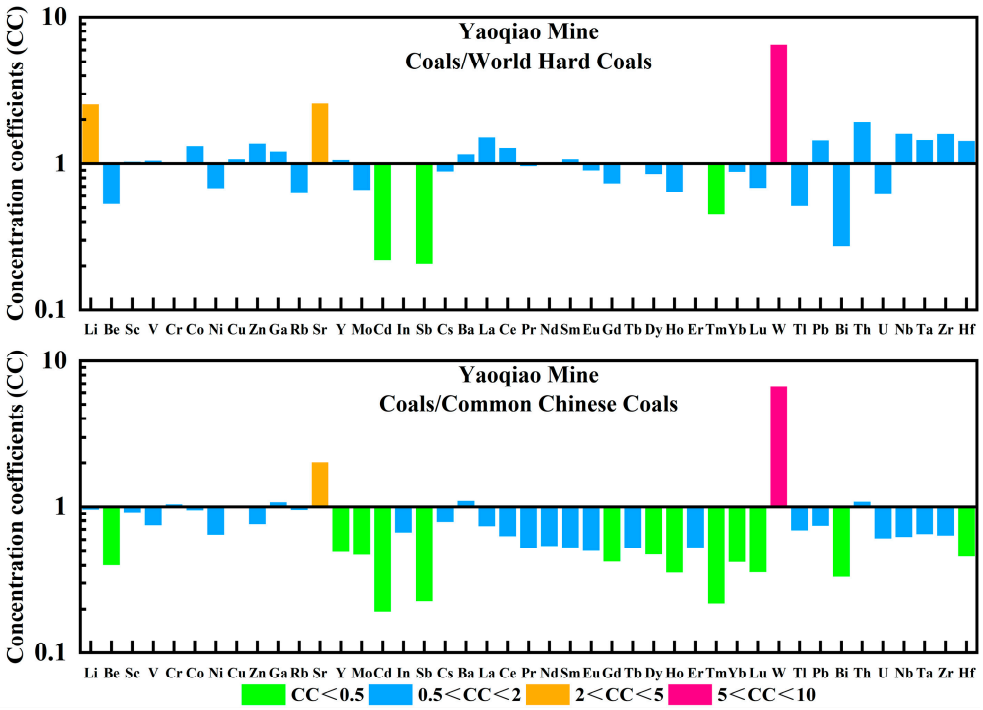


Figure 12. Concentration coefficients (CC) of trace elements in Yaoqiao mine samples (normalized to world coals and Chinese coals).

There were differences in the concentration coefficients of trace elements between the samples obtained from the Kongzhuang mine (Figure 13). In samples C1, C2, and C3, the concentration coefficients of most trace elements were in the normal range (0.5–2), slightly enriched (2–5) or enriched (5–10), including Li, V, Sr, Cu, Ga, and other elements. In samples C4, C5, C6, C7, and C8, the concentration coefficients of most trace elements were less than 0.2, which is the depleted range. Taking the most depleted C8 as an example, only W and Ce were slightly enriched, and the remaining trace elements were in the depleted range. Samples C9 and C10 were relatively normal compared with the previous samples, but the depleted trace elements still accounted for a certain proportion. Compared with other samples in Kongzhuang Mine, sample KZ-Y1 was more enriched or enriched in most trace elements. This may be due to its location on the roof of the coal seam, close to the surrounding rock. Later geological activities (e.g., fluid migration) may have led to a certain degree of enrichment in these elements [68,69].

The concentration coefficients of trace elements in each sample from Longdong Mine did not differ greatly (Figure 14). From C1 to C8, the contents of rare earth elements in the sample ranged from deficient to normal. Compared with other samples, sample LD-Y1 was strongly enriched in W and Co trace elements. As W can exist in the form of a complex (WO_4^-), it can migrate and enrich with the fluid, similarly to hydrothermal wolframite. Considering that Co is a pro-iron element, it is often associated with iron ore [70] and is a hot-water sedimentary iron–cobalt ore, indicating that Co has certain fluid activity. Therefore, the enrichment of Co in Longdong ore samples may also have been caused by fluid migration or other later geological activities rather than occurring primarily.

Except for the roof samples, there were slight differences between the concentration coefficients of trace elements in the samples from the Yaoqiao mine (Figure 15). Samples YQ-C1 and YQ-C2 were enriched or slightly enriched in Sr. C8 (near the roof) were enriched in Th, Nb, Ta, Zr, and Hf, which may have been affected by the geological activities of the roof and surrounding rock. In addition to the above two differences, most of the trace elements and rare earth elements in the samples from sample YQ-C1 to sample YQ-C8 were normal or depleted. Most of the elements in the roof sample YQ-Y2 were enriched or

slightly enriched, and the W element is very enriched, which may also be related to the later activity of geological fluid, as discussed above.

Through the correlation analysis between ash yield and different elemental contents, it was found that Cs, Mo, Rb, Cu, V, U, and other elements in the two high-ash content samples occur inorganic minerals. These elements of the other 14 samples are positively correlated to ash yield. The correlation plots are shown in Figure 16, indicating that the elements largely occur in organic matter. Therefore, most of these elements occur both in organic and inorganic matter.

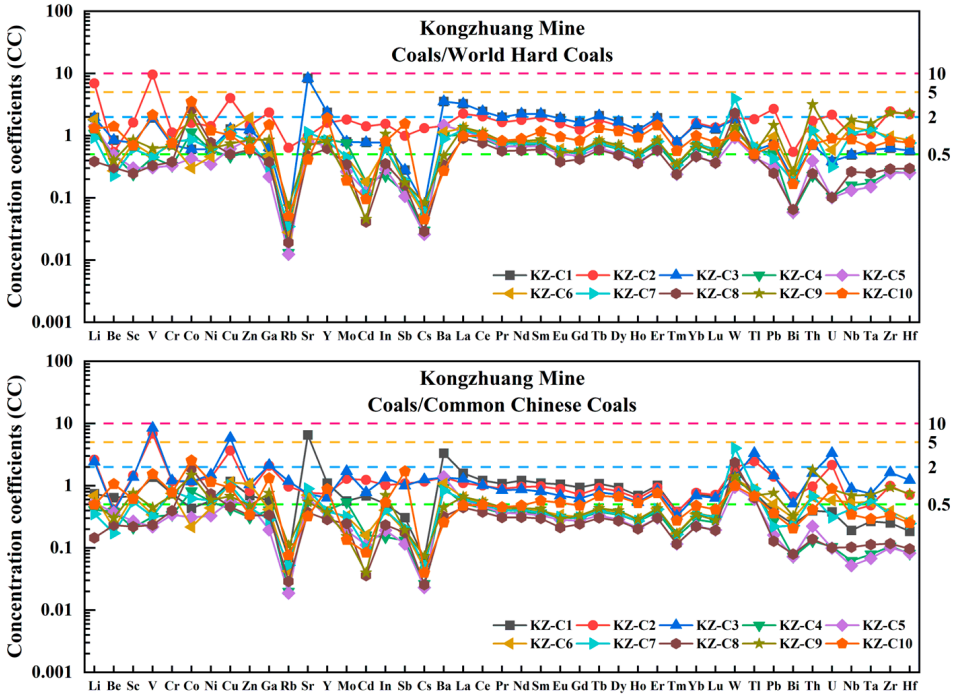


Figure 13. Concentration coefficients (CC) of trace elements in each sample from Kongzhuang Mine.

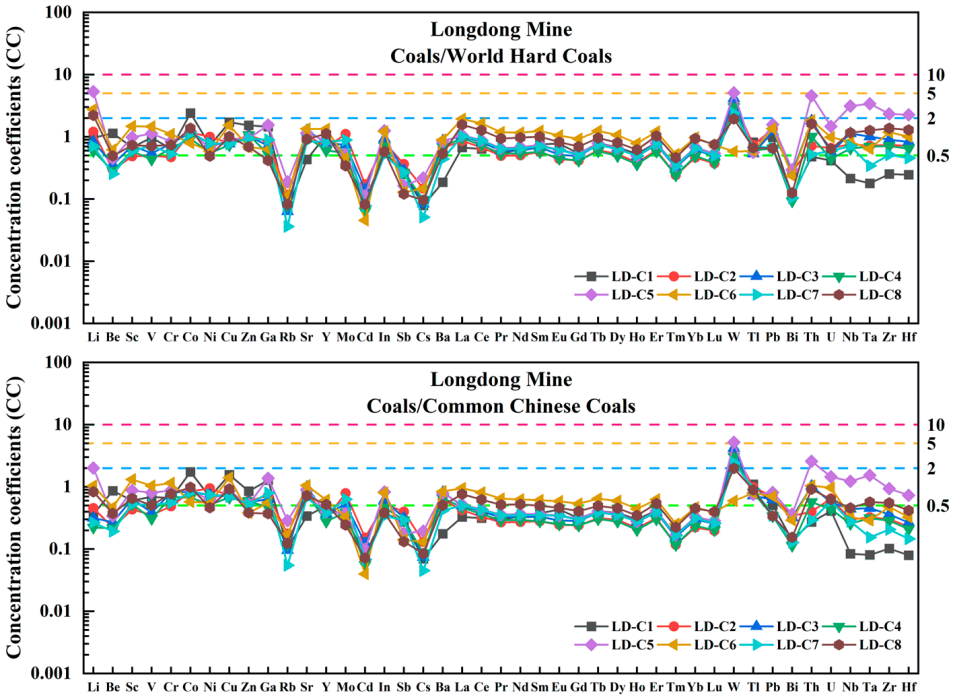


Figure 14. Concentration coefficients (CC) of trace elements in each sample from Longdong Mine.

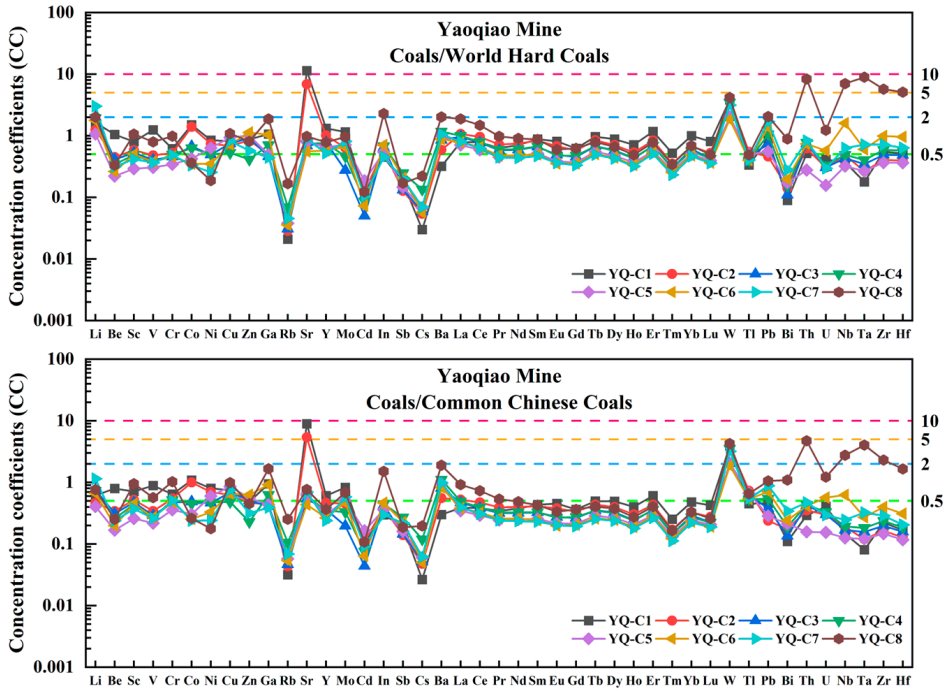


Figure 15. Concentration coefficients (CC) of trace elements in each sample from Yaoqiao Mine.

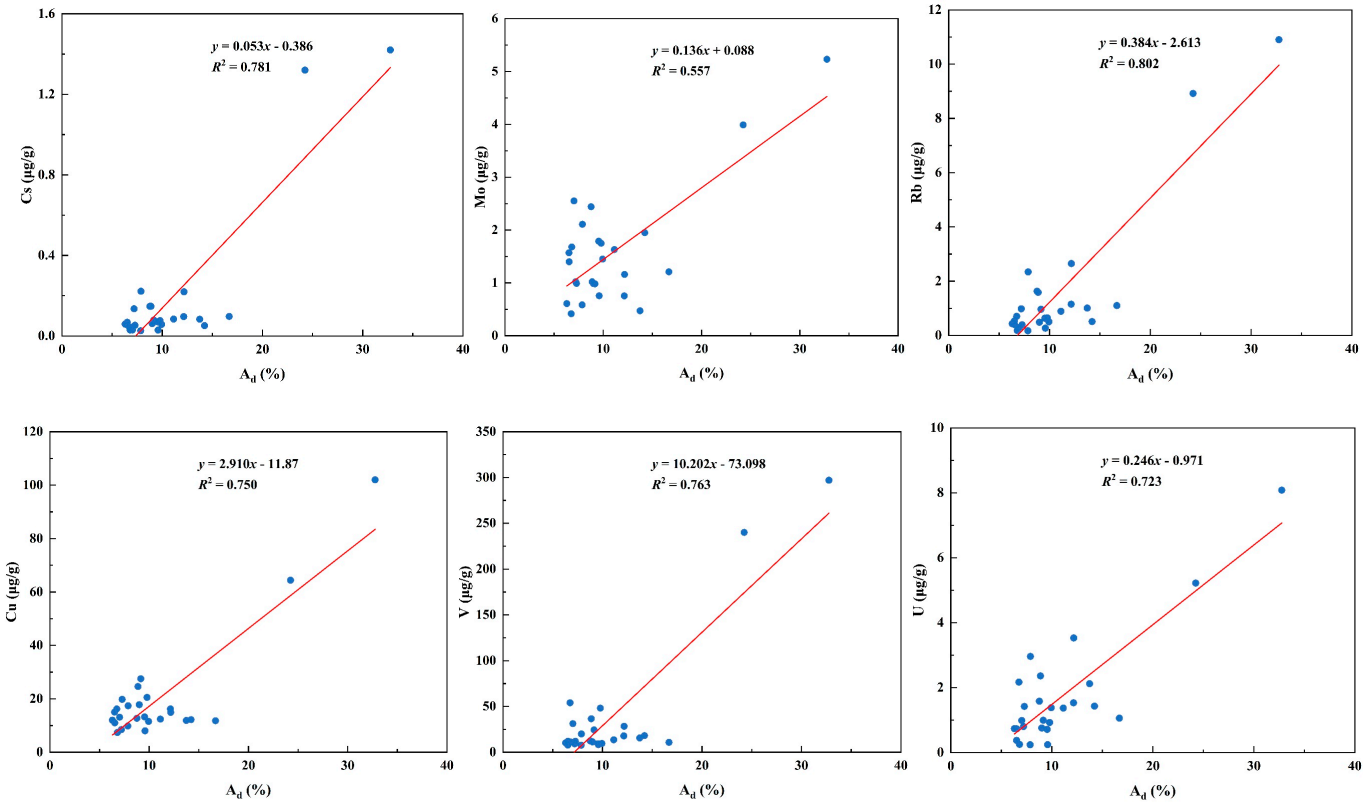


Figure 16. Correlation between different element concentrations and ash yields.

3.2.3. Rare Earth Elements

The REY data are provided in Table 3. The geochemical types of rare earth elements can be divided into three categories: light rare earth, medium rare earth, and heavy rare earth [71]. La, Ce, Pr, Nd, and Sm are light rare earth elements (LREY); Eu, Gd, Tb, Dy, and Y are medium rare earth elements (MREY); and Ho, Er, Tm, Yb, and Lu are heavy rare earth

elements (HREY) (Seredin and Dai, 2012). The corresponding rare earth element enrichment types can also be divided into light rare earth enrichment type ($La_N/Lu_N > 1$), medium rare earth enrichment type ($La_N/Sm_N < 1$; $Gd_N/Lu_N > 1$), and heavy rare earth enrichment type ($La_N/Lu_N < 1$) [71]. The rare earth elements in coal provide useful geochemical information on coal formation and related geological processes [72–76]. The rare earth elements in the coal sample from the Datun mining area are detailed in Table 4. According to the classification, the enrichment types of REY in all three coal mines were of L-type.

Table 3. Concentrations of rare earth elements and Y in the samples (μg/g).

Sample	La	Ce	Pr	Nd	Sm	Eu	Gd	Tb	Dy	Y	Ho	Er	Tm	Yb	Lu
KZ-C1	35.8	56.7	6.95	27	4.47	0.886	4.37	0.67	3.5	20	0.668	1.81	0.247	1.51	0.256
KZ-C2	24.8	46.9	5.74	21.4	3.96	0.742	3.36	0.57	3.06	13.5	0.596	1.67	0.241	1.6	0.271
KZ-C3	28.9	47.2	5.45	19.4	3.29	0.582	2.89	0.487	2.69	11.6	0.52	1.49	0.209	1.44	0.241
KZ-C4	11.5	20.5	2.32	8.38	1.47	0.259	1.4	0.235	1.28	7.31	0.256	0.676	0.097	0.595	0.097
KZ-C5	13	21.9	2.34	8.01	1.36	0.239	1.28	0.206	1.07	5.6	0.203	0.541	0.074	0.468	0.074
KZ-C6	14.6	24.7	2.68	9.18	1.59	0.283	1.47	0.252	1.44	7.05	0.278	0.777	0.109	0.749	0.121
KZ-C7	13.6	23.2	2.58	9.05	1.5	0.263	1.43	0.243	1.31	7.01	0.26	0.75	0.105	0.726	0.12
KZ-C8	10	17.6	1.98	6.94	1.21	0.178	1.13	0.189	1.02	5.22	0.194	0.542	0.074	0.461	0.073
KZ-C9	15	26.1	2.87	9.74	1.73	0.245	1.55	0.268	1.49	6.83	0.276	0.771	0.108	0.717	0.106
KZ-C10	10.8	23	2.89	10.7	2.34	0.448	2.24	0.425	2.48	16.1	0.504	1.36	0.176	0.995	0.158
KZ-Y1	65.6	112	13.7	53.1	9.54	1.91	8.49	1.41	7.58	37.3	1.51	4.29	0.615	4.1	0.682
LD-C1	7.41	14.7	1.91	7.5	1.53	0.364	1.46	0.253	1.43	9.03	0.288	0.75	0.101	0.627	0.1
LD-C2	9.46	15.6	1.73	6.07	1.14	0.206	1.12	0.196	1.11	5.71	0.209	0.566	0.075	0.463	0.075
LD-C3	11.2	18.8	2.08	7.22	1.36	0.242	1.32	0.239	1.4	6.73	0.263	0.7	0.1	0.624	0.097
LD-C4	10.5	17	1.87	6.54	1.14	0.211	1.12	0.189	1.04	5.07	0.196	0.543	0.075	0.491	0.077
LD-C5	11.7	20.3	2.29	8.2	1.48	0.289	1.44	0.252	1.38	7.22	0.267	0.736	0.108	0.681	0.108
LD-C6	21.4	37.9	4.16	14	2.49	0.492	2.5	0.4	2.23	11.2	0.424	1.13	0.163	0.975	0.148
LD-C7	11.3	19.9	2.24	7.83	1.42	0.29	1.38	0.24	1.33	6.92	0.268	0.711	0.105	0.657	0.099
LD-C8	17.2	29.2	3.3	11.7	2.02	0.386	1.89	0.307	1.7	9.47	0.334	0.965	0.144	0.938	0.151
LD-Y1	28.4	51.4	5.72	21	3.47	0.949	3.32	0.523	2.77	14.4	0.533	1.42	0.202	1.23	0.202
YQ-C1	8.71	18	2.2	8.47	1.76	0.383	1.69	0.309	1.85	11.1	0.386	1.09	0.162	1	0.161
YQ-C2	11.8	22.1	2.53	8.96	1.67	0.319	1.56	0.271	1.49	8.52	0.29	0.777	0.11	0.678	0.105
YQ-C3	10.6	17.8	2.04	7.12	1.33	0.231	1.23	0.218	1.22	6.61	0.236	0.635	0.093	0.602	0.086
YQ-C4	11	18.3	2.08	7.29	1.34	0.224	1.28	0.217	1.19	6.38	0.23	0.646	0.094	0.567	0.085
YQ-C5	7.81	13.6	1.58	5.6	1.04	0.181	1	0.177	0.997	5.51	0.2	0.522	0.085	0.5	0.079
YQ-C6	8.63	15.1	1.67	5.77	0.995	0.167	0.957	0.161	0.928	4.87	0.181	0.501	0.079	0.479	0.073
YQ-C7	8.82	14.4	1.56	5.25	0.941	0.17	0.902	0.158	0.896	4.39	0.173	0.475	0.072	0.463	0.072
YQ-C8	20.7	34.2	3.44	10.9	1.74	0.282	1.69	0.253	1.4	6.61	0.264	0.725	0.106	0.69	0.099
YQ-Y2	56	104	12.6	48.1	8.35	1.78	7.1	1.08	5.67	25.2	1.07	3.02	0.435	2.84	0.458

Table 4. Rare earth element parameters of samples.

Mine	Sample	La_N	Sm_N	Gd_N	Lu_N	La_N/Sm_N	La_N/Lu_N	Gd_N/Lu_N
Kongzhuang	KZ-7-C1	151.05	29.22	21.27	10.08	5.17	14.99	2.11
	KZ-7-C2	104.64	25.88	16.35	10.67	4.04	9.81	1.53
	KZ-7-C3	121.94	21.50	14.06	9.49	5.67	12.85	1.48
	KZ-7-C4	48.52	9.61	6.81	3.82	5.05	12.71	1.78
	KZ-7-C5	54.85	8.89	6.23	2.91	6.17	18.83	2.14
	KZ-7-C6	61.60	10.39	7.15	4.76	5.93	12.93	1.50
	KZ-7-C7	57.38	9.80	6.96	4.72	5.85	12.15	1.47
	KZ-7-C8	42.19	7.91	5.50	2.87	5.34	14.68	1.91
	KZ-7-C9	63.29	11.31	7.54	4.17	5.60	15.17	1.81
	KZ-7-C10	45.57	15.29	10.90	6.22	2.98	7.33	1.75
	KZ-D-Y1	276.79	62.35	41.31	26.85	4.44	10.31	1.54
Longdong	LD-7-C1	31.27	10.00	7.10	3.94	3.13	7.94	1.80
	LD-7-C2	39.92	7.45	5.45	2.95	5.36	13.52	1.85
	LD-7-C3	47.26	8.89	6.42	3.82	5.32	12.37	1.68
	LD-7-C4	44.30	7.45	5.45	3.03	5.95	14.61	1.80
	LD-7-C5	49.37	9.67	7.01	4.25	5.10	11.61	1.65
	LD-7-C6	90.30	16.27	12.17	5.83	5.55	15.50	2.09
	LD-7-C7	47.68	9.28	6.72	3.90	5.14	12.23	1.72
	LD-7-C8	72.57	13.20	9.20	5.94	5.50	12.21	1.55
	LD-D-Y1	119.83	22.68	16.16	7.95	5.28	15.07	2.03

Table 4. *Cont.*

Mine	Sample	La_N	Sm_N	Gd_N	Lu_N	La_N/Sm_N	La_N/Lu_N	Gd_N/Lu_N
Yaoqiao	YQ-7-C1	36.75	11.50	8.22	6.34	3.19	5.80	1.30
	YQ-7-C2	49.79	10.92	7.59	4.13	4.56	12.04	1.84
	YQ-7-C3	44.73	8.69	5.99	3.39	5.15	13.21	1.77
	YQ-7-C4	46.41	8.76	6.23	3.35	5.30	13.87	1.86
	YQ-7-C5	32.95	6.80	4.87	3.11	4.85	10.60	1.56
	YQ-7-C6	36.41	6.50	4.66	2.87	5.60	12.67	1.62
	YQ-7-C7	37.22	6.15	4.39	2.83	6.05	13.13	1.55
	YQ-7-C8	87.34	11.37	8.22	3.90	7.68	22.41	2.11
	YQ-D-Y2	236.29	54.58	34.55	18.03	4.33	13.10	1.92

The REY distribution patterns for each deposit are shown in Figures 17–19, where the UCC-normalized data are quoted from Taylor and McLennan [77]. The distribution curves for Kongzhuang mine, Longdong mine, and Yaoqiao mine can be seen to be inclined to the right, with a negative Eu anomaly (Eu anomaly was calculated based on the formula proposed by Dai et al. [78]), and the enrichment type is the light rare earth enrichment type. Among them, the total rare earth content in Kongzhuang mine samples was ∑REE = 41.6–284.5 μg/g, where the rare earth concentrations in samples KZ-C1, KZ-C2, KZ-C3, and KZ-Y1 were higher than those in other samples (between 114.9 and 284.5 μg/g); the total concentration of rare earth elements in Longdong mine samples was ∑REE = 38.4–121.1 μg/g, where the concentration of rare earth elements in sample LD-Y1 was higher (121.1 μg/g); and the total concentration of rare earth elements in the Yaoqiao mine samples was ∑REE = 33.4–252.5 μg/g, where the rare earth element concentration in sample YQ-Y2 was significantly higher than those in other samples (252.5 μg/g)—excluding this sample, the ∑REE for the other samples was 33.4–76.5 μg/g.

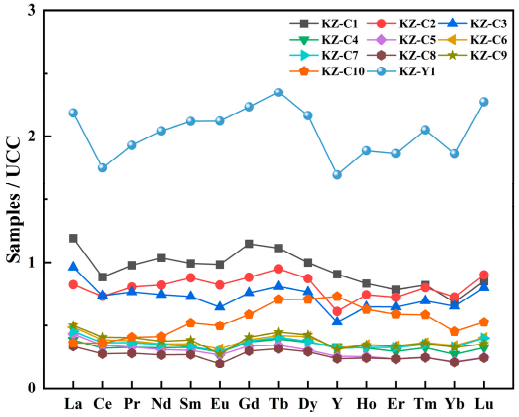


Figure 17. REY distribution patterns in Kongzhuang Mine samples [77].

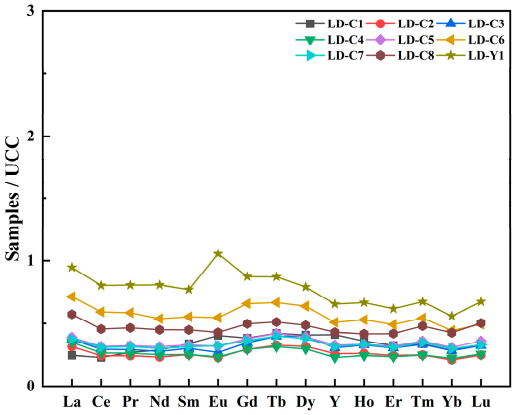


Figure 18. REY distribution patterns in Longdong Mine samples [77].

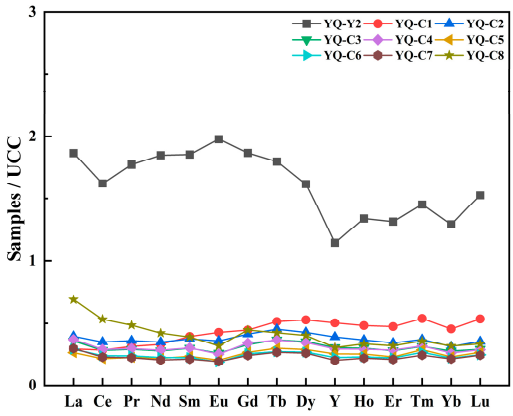


Figure 19. REY distribution patterns in Yaoqiao Mine samples [77].

In the process of geochemical action, the +2 valence Eu will be separated from other +3 valence element ions under high-temperature and reducing conditions [29], resulting in a valley in the position of Eu in the UCC-normalized patterns, and Eu depleted, which presents a negative anomaly. As shown in Figures 17–19, Eu in Kongzhuang, Longdong, and Yaoqiao Mine samples showed strong negative anomalies, which may be related to the materials derived from the sediment source region. This also indicated that the later sedimentary environment was not strongly changed by factors such as seawater and magma. Variation of rare earth element Eu in Kongzhuang, Longdong, and Yaoqiao Mine samples was shown in Figure 20. The factors controlling Eu anomalies in coal include the parent rock properties of the sedimentary source area [79] and the influence of high-temperature hydrothermal fluids plus reducing conditions [29].

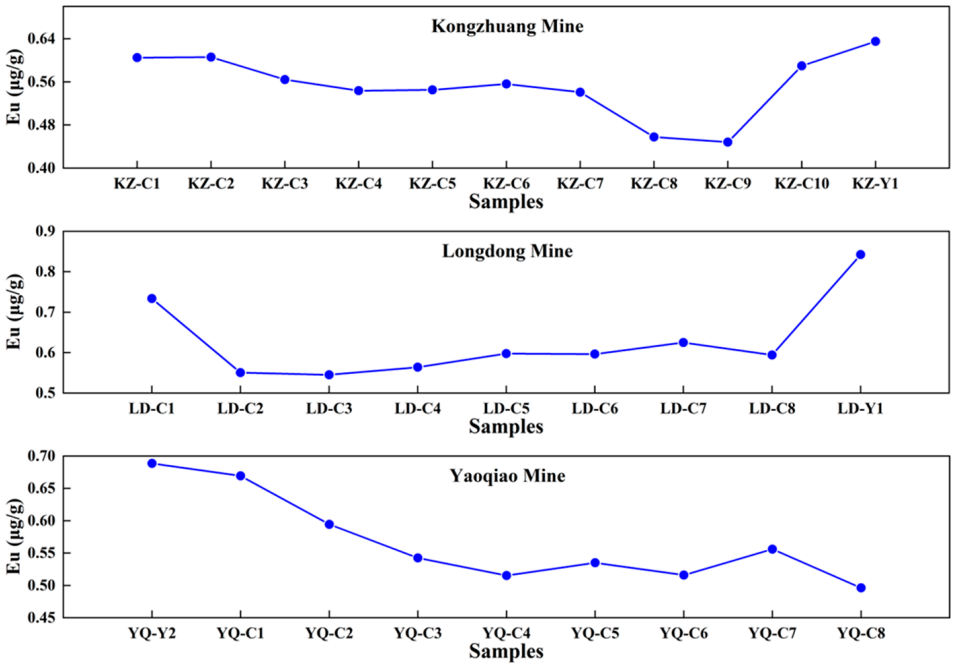


Figure 20. Variation of rare earth element Eu in Kongzhuang, Longdong, and Yaoqiao Mine samples (μg/g).

3.3. Modes of Occurrence of Pb and Pb Isotopes

The combination relationships between associated elements and trace elements in coal were studied through systematic clustering. The statistical method used for cluster analysis was the similarity matrix, and the clustering method was an inter-group connection. The correlations between intervals were calculated according to Pearson correlations. The

values were normalized to a maximum value of 1, and two groups were obtained with a similarity distance of 15, as shown in Figure 21.

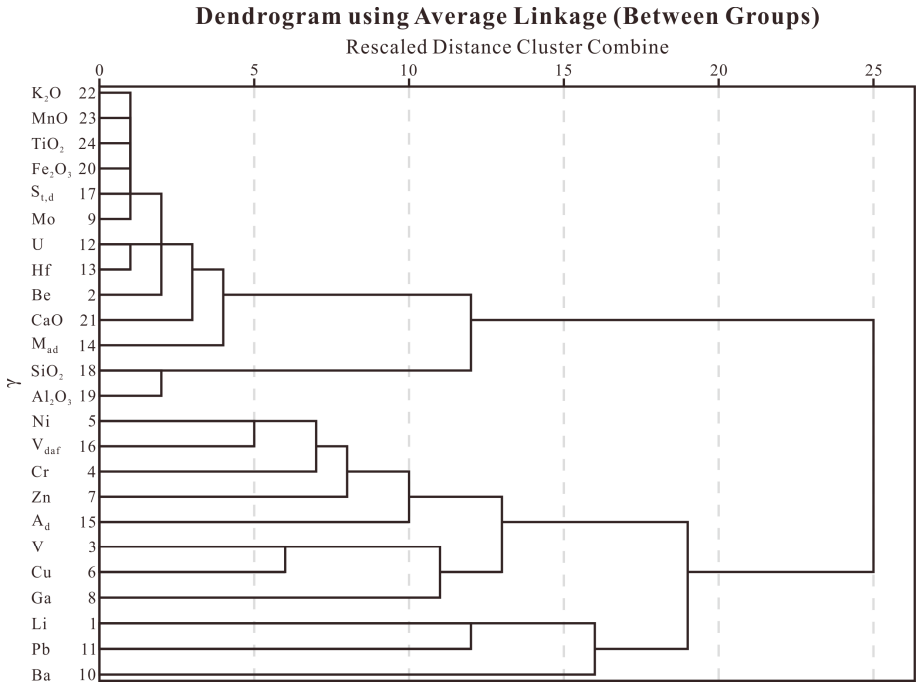


Figure 21. Cluster analysis diagram.

Group 1 included K_2O, TiO_2, Fe_2O_3, $S_{t.d}$, Mo, Hf, U, Be, CaO, SiO_2, and Al_2O_3. This group mainly consists of lithophile and siderophile elements and also contains SiO_2 and Al_2O_3, which are the major elements of clay minerals. Many researchers [80,81] have studied the occurrence of MnO in coal, mainly in the following ways: occurrence in carbonate minerals in the form of isomorphism, including calcite and dolomite; in the form of adsorption in clay minerals; occurrence in pyrite, as associated elements of pyrite [1], combined with organic functional groups in the form of organic state, mainly in low-rank coal [82], and in a very few cases, in alabandite [28]. In most coals, the main form of Ti is the ubiquitous Ti oxide, although a large amount of TiO_2 may be related to clay (e.g., kaolinite [63]). In low-rank coal, TiO_2 may be mainly associated with organic matter [54,55,83]. There are many forms of Fe_2O_3, which can occur in both clay and sulfide minerals [1]. Be is generally present in organic matter and clay minerals, and in some cases, it occurs in Be-bearing sulfates [84], but Be present in samples of this study is not located in a group with volatiles but, instead, in the group with total sulfur, indicating that Be is typically present in sulfides, and not in organic matter. The mode of occurrence of CaO depends partly on the grade of coal. In bituminous coal and anthracite, CaO is usually present in carbonates; however, in low-rank coal (lignite and subbituminous coal), there may be more organically bound CaO [18,83].

Group 2, including Ni, Cr, Zn, ash, V, Cu, Ga, Li, Ba, Pb, Ni, V, Cr, and Zn, is mainly present in inorganic minerals and organic matter. Cu in coal mainly exists in chalcopyrite and pyrite and may exist in the organic matter of some low-rank coals. Early studies [5] have shown that Ga in coal has a strong organic affinity, and it has been found that Ga is related to aluminosilicate. Li seems to be mainly related to silicates in high- and low-rank coals [35,85–87]. Ba is a lithophile element, and its occurrence state in coal is diverse. The main occurrence modes of Ba are as follows: 1. replacing K_2O in clay minerals as an isomorphic form; 2. in the form of organic matter; and (3) existing in the form of barite ($BaCO_3$), barite ($BaSO_4$), lepidocrocite, and other minerals [88–91]. Lead in coal is mainly present in pyrite and, in some cases, in trace minerals (e.g., galena) and organic matter [1,92,93].

3.4. Pb Isotope Characteristics

The Pb isotope composition of coal samples from the Datun mining area is shown in Table 5. The $^{208}Pb/^{204}Pb$ in Kongzhuang mine samples was between 37.731 and 39.655, the $^{207}Pb/^{204}Pb$ was between 15.345 and 15.629, and the $^{206}Pb/^{204}Pb$ was between 17.315 and 18.867. The $^{208}Pb/^{204}Pb$ in Longdong mine samples was between 37.602 and 38.764, the $^{207}Pb/^{204}Pb$ was between 15.430 and 15.583, and the $^{206}Pb/^{204}Pb$ was between 17.251 and 18.562. The $^{208}Pb/^{204}Pb$ in Yaoqiao mine samples was between 37.776 and 38.942, the $^{207}Pb/^{204}Pb$ was between 15.411 and 15.583, and the $^{206}Pb/^{204}Pb$ was between 17.705 and 18.579. The standard deviations of $^{208}Pb/^{204}Pb$, $^{207}Pb/^{204}Pb$, and $^{206}Pb/^{204}Pb$ in the three mine samples were 0.005–0.015, 0.001–0.005, and 0.001–0.006, respectively. These values can be used to trace the source of the ore-forming materials.

Table 5. Lead isotope composition of the Datun mining area samples.

Mine	Sample	$^{208}Pb/^{204}Pb$	Std err	$^{207}Pb/^{204}Pb$	Std err	$^{206}Pb/^{204}Pb$	Std err	Δβ	Δγ
Kongzhuang	KZ-C1	38.435	0.005	15.604	0.002	18.496	0.002	18.604	35.481
	KZ-C2	37.979	0.009	15.523	0.003	18.217	0.004	13.316	23.196
	KZ-C3	38.226	0.007	15.567	0.003	17.882	0.004	16.189	29.850
	KZ-C4	37.767	0.007	15.457	0.003	17.73	0.003	9.008	17.484
	KZ-C5	38.299	0.012	15.487	0.004	18.065	0.005	10.966	31.817
	KZ-C6	38.386	0.007	15.548	0.003	18.322	0.003	14.948	34.161
	KZ-C7	39.655	0.007	15.629	0.003	18.867	0.003	20.236	68.349
	KZ-C8	38.049	0.007	15.488	0.002	18.039	0.003	11.032	25.082
	KZ-C9	37.731	0.005	15.345	0.002	17.315	0.002	1.697	16.514
	KZ-C10	37.768	0.005	15.351	0.002	17.374	0.002	2.088	17.511
	KZ-Y1	38.391	0.006	15.513	0.002	18.116	0.003	12.664	34.296
Longdong	LD-C1	38.281	0.013	15.583	0.005	18.26	0.006	17.233	31.332
	LD-C2	38.764	0.015	15.559	0.004	18.526	0.005	15.666	44.345
	LD-C3	38.089	0.003	15.518	0.002	18.351	0.002	12.990	26.159
	LD-C4	38.347	0.004	15.508	0.002	18.15	0.002	12.337	33.110
	LD-C5	38.423	0.005	15.43	0.002	17.621	0.002	7.245	35.158
	LD-C6	38.607	0.007	15.547	0.002	18.469	0.003	14.883	40.115
	LD-C7	38.754	0.005	15.566	0.002	18.338	0.002	16.123	44.075
	LD-C8	38.271	0.003	15.56	0.001	18.35	0.001	15.732	31.063
	LD-Y1	37.602	0.005	15.438	0.002	17.251	0.002	7.768	13.039
Yaoqiao	YQ-C1	38.165	0.008	15.545	0.003	18.256	0.003	14.752	28.207
	YQ-C2	38.678	0.004	15.583	0.002	18.579	0.002	17.233	42.028
	YQ-C3	38.686	0.003	15.59	0.001	18.56	0.001	17.690	42.243
	YQ-C4	38.34	0.005	15.545	0.002	18.221	0.003	14.752	32.922
	YQ-C5	38.127	0.005	15.539	0.002	18.083	0.002	14.361	27.183
	YQ-C6	37.835	0.007	15.463	0.003	17.752	0.003	9.400	19.316
	YQ-C7	37.776	0.003	15.459	0.001	17.705	0.001	9.138	17.727
	YQ-C8	38.942	0.005	15.411	0.002	17.642	0.002	6.005	49.140
	YQ-Y2	38.339	0.009	15.574	0.003	17.834	0.003	16.645	32.895

Figure 22 shows that there is a good linear relationship between different lead isotope ratios, indicating that the Pb source in this area is relatively singular, with a common Pb source.

The composition of lead isotopes plays an important role in tracing the source of ore-forming materials. If the geological body does not contain or contains a small amount of radioactive lead, the lead isotopes in the geological body can determine the source of the ore-forming materials [94]. In the $^{208}Pb/^{204}Pb$–$^{206}Pb/^{204}Pb$ tectonic model diagram (Figure 23a), the sample points for Kongzhuang and Longdong mines are mainly cast between the orogenic belt and the upper crust, and most of the Yaoqiao mine sample points are also distributed between the orogenic belt and the upper crust, with only sample YQ-C8 falling on the boundary between the orogenic belt and the lower crust source area. In the $^{207}Pb/^{204}Pb$–$^{206}Pb/^{204}Pb$ tectonic model diagram (Figure 23b), the lead isotope values

of the sample points in the three mining areas cut through the growth curves of the two lead source areas of the orogenic belt and the mantle. The span of the samples from the Kongzhuang mine is large, and the distribution of sample points ranges from the growth curve of the lead source area of the orogenic belt to that of the lead source area close to the lower crust. Compared with the Kongzhuang mine sample points, the distributions of Longdong and Yaoqiao mine sample points are more concentrated, with almost all falling between the orogenic belt and mantle lead source growth curves, suggesting that Longdong mine and Yaoqiao mine have the same source or evolution process. There is an obvious linear trend in the distribution of lead isotopes in Longdong and Yaoqiao mines, which is usually considered to be characteristic of a mixed source of Pb.

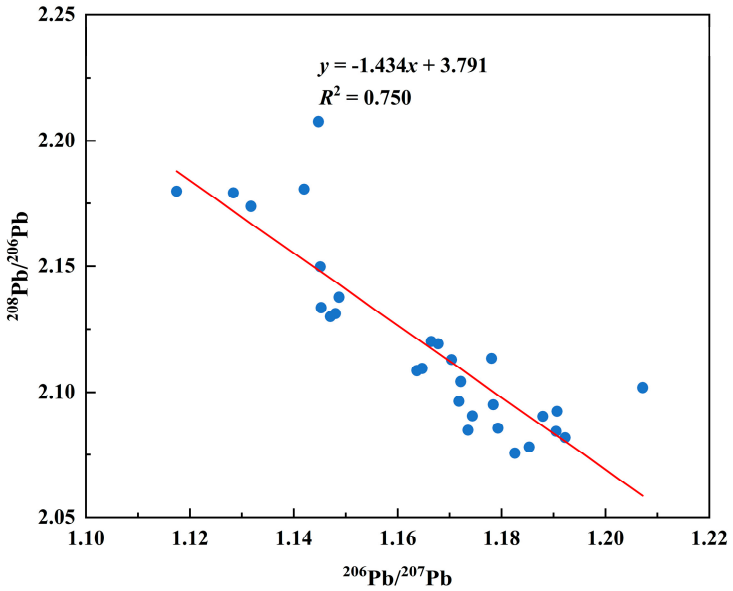


Figure 22. $^{206}Pb/^{207}Pb$ and $^{208}Pb/^{206}Pb$ scatter diagram.

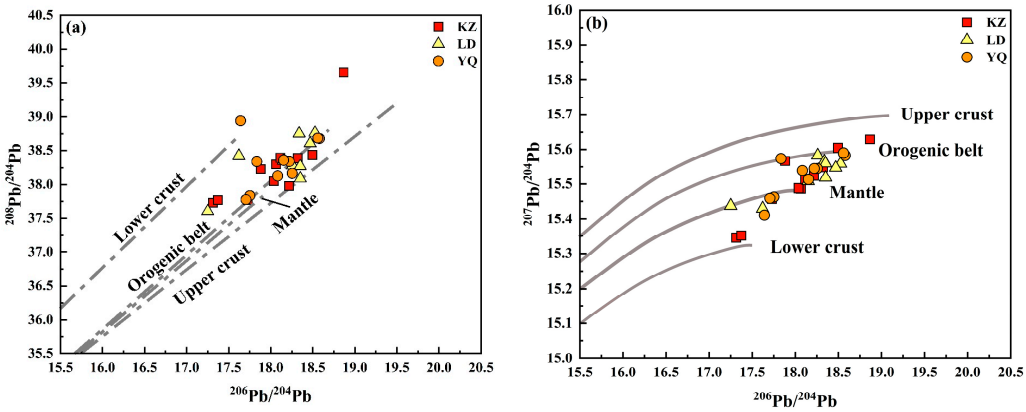


Figure 23. Lead isotope structure model diagram for the Datun mining area; base map according to Zartman and Doe [95]. (**a**) diagram of $^{206}Pb/^{204}Pb$ and $^{208}Pb/^{204}Pb$; (**b**) diagram of $^{206}Pb/^{204}Pb$ and $^{207}Pb/^{204}Pb$.

In the genetic classification diagram of lead isotope $\Delta\beta$-$\Delta\gamma$ in the Datun mining area (Figure 24), the three deposits are mainly distributed in the orogenic and subduction zone lead source areas mixed with the upper crust and mantle, where individual sample points are distributed in the mantle and upper crust lead source areas. Based on the above three lead isotope source discrimination diagrams, it can be considered that the lead of the samples in the three mining areas mainly derives from the orogenic belt and the crust–

mantle mixed subduction zone. Furthermore, there are also lead additions from upper crust and mantle sources.

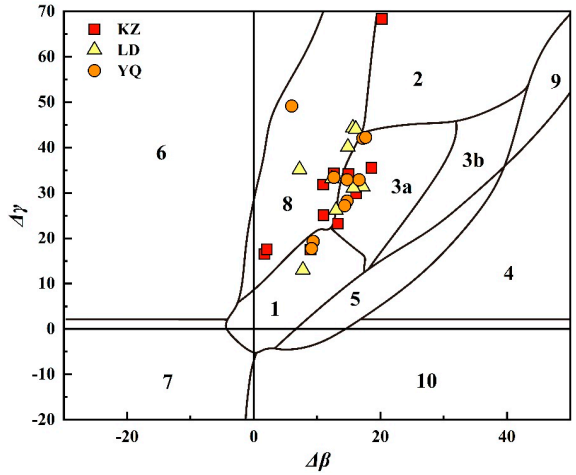


Figure 24. The genetic classification diagram of lead isotope $\Delta\beta$-$\Delta\gamma$ in the Datun mining area. 1, mantle source lead; 2, Upper crust lead; 3, Upper crust and mantle mixed subduction zone lead (3a, magmatism; 3b, sedimentation); 4, chemically deposited lead; 5, Submarine hot water acting on lead; 6, medium-deep metamorphic lead; 7, deep metamorphic lead; 8, orogenic lead; 9, old shale upper crust lead; 10, deteriorated lead, according to Zartman and Doe [95].

4. Conclusions

(1) The major minerals in the thick coal seam of the Datun mining area are clay minerals, calcite, quartz, and dolomite; SiO_2 and Al_2O_3 are mainly in the form of clay minerals, and there is a good correlation between them. Fe is mainly in the form of pyrite, and Ca is mainly in the form of calcite;

(2) The samples from Kongzhuang, Longdong, and Yaoqiao mines basically fall in the felsic source area, so it is considered that the sediment source in the study area is felsic source rock;

(3) There are differences in the enrichment degree of trace elements between the Kongzhuang mine, Longdong mine, and Yaoqiao mine samples. Compared with the average values of elements in coal in the world, Li and W elements were found to be enriched as a whole. In particular, W was enriched in the Yaoqiao mine and highly enriched in Longdong mine samples. The distribution curve of rare earth elements in the three mines is inclined to the right overall, indicating the light rare earth enrichment type;

(4) The lead in the coal samples from the Datun mining area mainly exists in pyrite, and there is little radioactive lead. There is a good correlation between $^{206}Pb/^{207}Pb$ and $^{208}Pb/^{206}Pb$, indicating that the source of Pb in this area is relatively singular, mainly from the orogenic belt and crust–mantle mixed subduction zone, as well as some upper crust and mantle source areas.

Author Contributions: N.M.: methodology, writing—review; Q.X.: formal analysis and data curation. W.L.: supervision, visualization. All authors have read and agreed to the published version of the manuscript.

Funding: This research was funded by the Major Science and Technology Special Project of Xinjiang Uygur Autonomous Region (No. 2022A03014-2) and the Natural Science Foundation of the Jiangsu Higher Education Institutions of China (No. 23KJA610006).

Data Availability Statement: The data are available on request from the corresponding author.

Conflicts of Interest: The authors declare that they have no known competing financial interests or personal relationships that could have appeared to influence the work reported in the paper.

References

1. Dai, S.; Finkelman, R.B.; French, D.; Hower, J.C.; Graham, I.T.; Zhao, F. Modes of occurrence of elements in coal: A critical evaluation. *Earth-Sci. Rev.* **2021**, *222*, 103815. [CrossRef]
2. Tuncer, A.; Karayigit, A.I.; Oskay, R.G.; Tunoğlu, C.; Kayseri-Özer, M.S.; Gümüş, B.A.; Bulut, Y.; Akbulut, A. A multi-proxy record of palaeoenvironmental and palaeoclimatic conditions during Plio-Pleistocene peat accumulation in the eastern flank of the Isparta Angle: A case study from the Şarkikaraağaç coalfield (Isparta, SW Central Anatolia). *Int. J. Coal Geol.* **2023**, *265*, 104149. [CrossRef]
3. Zdravkov, A.; Groß, D.; Bechtel, A.; Stojanović, K.; Kojić, I. Depositional settings of the Eocene Suhostrel bituminous coal, SW Bulgaria, inferred from organic petrology and molecular proxies. *Int. J. Coal Geol.* **2023**, *276*, 104319. [CrossRef]
4. Li, X.; Zhuang, X.G.; Zhou, J.B.; Wang, H.; Ma, X.P. Coal facies analysis of thick coal seam of middle Jurassic Xishanyao Formation in the middle part of eastern Junggar coal field, Xinjiang. Geol. *Sci. Tech* **2010**, *29*, 84–88.
5. Liu, J.; Spiro, B.F.; Dai, S.; French, D.; Graham, I.T.; Wang, X.; Zhao, L.; Zhao, J.; Zeng, R. Strontium isotopes in high-and low-Ge coals from the Shengli Coalfield, Inner Mongolia, northern China: New indicators for Ge source. *Int. J. Coal Geol.* **2021**, *233*, 103642. [CrossRef]
6. Spiro, B.F.; Liu, J.; Dai, S.; Zeng, R.; Large, D.; French, D. Marine derived $^{87}Sr/^{86}Sr$ in coal, a new key to geochronology and palaeoenvironment: Elucidation of the India-Eurasia and China-Indochina collisions in Yunnan, China. *Int. J. Coal Geol.* **2019**, *215*, 103304. [CrossRef]
7. Shao, L.; Dang, X.; Gao, X.; Wang, D.; Wen, H.; Wang, X.; Cao, D.; Lu, J. Genetic mechanism of thick coal seams: Astronomical-forcing superimposed multi-staged swamp model. *Coal Sci. Technol.* **2022**, *50*, 186–195.
8. Hower, J.C.; Finkelman, R.B.; Eble, C.F.; Arnold, B.J. Understanding coal quality and the critical importance of comprehensive coal analyses. *Int. J. Coal Geol.* **2022**, *263*, 104120. [CrossRef]
9. Hower, J.C.; Gebremedhin, M.; Zourarakis, D.P.; Finkelman, R.B.; French, D.; Graham, I.T.; Schobert, H.H.; Zhao, L.; Dai, S. Is hyperaccumulation a viable hypothesis for organic associations of minor elements in coals? *Earth-Sci. Rev.* **2024**, *254*, 104802. [CrossRef]
10. Dai, S.; Bechtel, A.; Eble, C.F.; Flores, R.M.; French, D.; Graham, I.T.; Hood, M.M.; Hower, J.C.; Korasidis, V.A.; Moore, T.A.; et al. Recognition of peat depositional environments in coal: A review. *Int. J. Coal Geol.* **2020**, *219*, 103383.
11. Dai, S.; Hower, J.C.; Finkelman, R.B.; Graham, I.T.; French, D.; Ward, C.R.; Eskenazy, G.; Wei, Q.; Zhao, L. Organic associations of non-mineral elements in coal: A review. *Int. J. Coal Geol.* **2020**, *218*, 103347. [CrossRef]
12. Dai, S.; Finkelman, R.B.; Hower, J.C.; French, D.; Graham, I.T.; Zhao, L. *Inorganic Geochemistry of Coal*; Elsevier: Amsterdam, The Netherlands, 2023.
13. Dai, S.; Yan, X.; Ward, C.R.; Hower, J.C.; Zhao, L.; Wang, X.; Zhao, L.; Ren, D.; Finkelman, R.B. Valuable elements in Chinese coals: A review. *Int. Geol. Rev.* **2018**, *60*, 590–620. [CrossRef]
14. Dai, S.; Finkelman, R.B. Coal as a promising source of critical elements: Progress and future prospects. *Int. J. Coal Geol.* **2018**, *186*, 155–164. [CrossRef]
15. Di, S.; Dai, S.; Nechaev, V.P.; French, D.; Graham, I.T.; Zhao, L.; Finkelman, R.B.; Wang, H.; Zhang, S.; Hou, Y. Mineralogy and enrichment of critical elements (Li and Nb-Ta-Zr-Hf-Ga) in the Pennsylvanian coals from the Antaibao Surface Mine, Shanxi Province, China: Derivation of pyroclastics and sediment-source regions. *Int. J. Coal Geol.* **2023**, *273*, 104262. [CrossRef]
16. Di, S.; Dai, S.; Nechaev, V.P.; Zhang, S.; French, D.; Graham, I.T.; Spiro, B.; Finkelman, R.B.; Hou, Y.; Wang, Y.; et al. Granite-bauxite provenance of abnormally enriched boehmite and critical elements (Nb, Ta, Zr, Hf and Ga) in coals from the Eastern Surface Mine, Ningwu Coalfield, Shanxi Province, China. *J. Geochem. Explor.* **2022**, *239*, 107016. [CrossRef]
17. Liu, J.; Dai, S.; Berti, D.; Eble, C.F.; Dong, M.; Gao, Y.; Hower, J.C. Rare Earth and Critical Element Chemistry of the Volcanic Ash-fall Parting in the Fire Clay Coal, Eastern Kentucky, USA. *Clays Clay Miner.* **2023**, *71*, 309–339. [CrossRef]
18. Moore, T.A.; Dai, S.; Huguet, C.; Pearse, J.; Liu, J.; Esterle, J.S.; Jia, R. Petrographic and geochemical characteristics of selected coal seams from the late Cretaceous-Paleocene Guaduas Formation, Eastern Cordillera Basin, Colombia. *Int. J. Coal Geol.* **2022**, *259*, 104042. [CrossRef]
19. Wang, Q.; Dai, S.; French, D.; Spiro, B.; Graham, I.; Liu, J. Hydrothermally-altered coal from the Daqingshan Coalfield, Inner Mongolia, northern China: Evidence from stable isotopes of C within organic matter and C-O-Sr in associated carbonates. *Int. J. Coal Geol.* **2023**, *276*, 104330. [CrossRef]
20. Chatterjee, S.; Karacan, C.Ö.; Mastalerz, M. Exploring the uncertainty of machine learning models and geostatistical mapping of rare earth element potential in Indiana coals, USA. *Int. J. Coal Geol.* **2024**, *282*, 104419. [CrossRef]
21. Du, F.; Qiao, J.; Zhao, X.; Tan, F.; Li, C.; Luo, Z. Enrichment of V in Late Permian coals in Gemudi Mine, Western Guizhou, SW China. *J. Geochem. Explor.* **2021**, *221*, 106701. [CrossRef]
22. Jiu, B.; Huang, W.; Spiro, B.; Hao, R.; Mu, N.; Wen, L.; Hao, H. Distribution of Li, Ga, Nb, and REEs in coal as determined by LA-ICP-MS imaging: A case study from Jungar coalfield, Ordos Basin, China. *Int. J. Coal Geol.* **2023**, *267*, 104184. [CrossRef]
23. Dai, S.; Ren, D.; Tang, Y.; Yue, M.; Hao, L.M. Concentration and distribution of elements in Late Permian coals from western Guizhou Province, China. *Int. J. Coal Geol.* **2005**, *61*, 119–137. [CrossRef]
24. Liu, Z.; Wei, Y.; Ning, S.; Jia, X.; Qin, R.; Cao, D. The differences of element geochemical characteristics of the main coal seams in the Ningdong coalfield, Ordos Basin. *J. Geochem. Explor.* **2019**, *202*, 77–91.

25. Zhou, M.; Zhao, L.; Wang, X.; Nechaev, V.P.; French, D.; Spiro, B.F.; Hower, J.; Dai, S. Mineralogy and geochemistry of the Late Triassic coal from the Caotang mine, northeastern Sichuan Basin, China, with emphasis on the enrichment of the critical element lithium. *Ore Geol. Rev.* **2021**, *139*, 104582. [CrossRef]
26. Mishra, V.; Chakravarty, S.; Finkelman, R.B.; Varma, A.K. Geochemistry of rare earth elements in lower Gondwana coals of the Talchir Coal Basin, India. *J. Geochem. Explor.* **2019**, *204*, 43–56. [CrossRef]
27. Equeenuddin, S.M.; Tripathy, S.; Sahoo, P.K.; Ranjan, A. Geochemical characteristics and mode of occurrence of trace elements in coal at West Bokaro coalfield. *Int. J. Coal Sci. Technol.* **2016**, *3*, 399–406. [CrossRef]
28. Dai, S.; Xie, P.; Jia, S.; Ward, C.R.; Hower, J.C.; Yan, X.; French, D. Enrichment of U-Re-V-Cr-Se and rare earth elements in the Late Permian coals of the Moxinpo Coalfield, Chongqing, China: Genetic implications from geochemical and mineralogical data. *Ore Geol. Rev.* **2017**, *80*, 1–17. [CrossRef]
29. Dai, S.; Ji, D.; Ward, C.R.; French, D.; Hower, J.C.; Yan, X.; Wei, Q. Mississippian anthracites in Guangxi Province, southern China: Petrological, mineralogical, and rare earth element evidence for high-temperature solutions. *Int. J. Coal Geol.* **2018**, *197*, 84–114. [CrossRef]
30. Nechaev, V.P.; Bechtel, A.; Dai, S.; Chekryzhov, I.Y.; Pavlyutkin, B.I.; Vysotskiy, S.V.; Ignatiev, A.V.; Velivetskaya, T.A.; Guo, W.; Tarasenko, I.A.; et al. Bio-geochemical evolution and critical element mineralization in the Cretaceous-Cenozoic coals from the southern Far East Russia and northeastern China. *Appl. Geochem.* **2020**, *117*, 104602. [CrossRef]
31. Arbuzov, S.I.; Chekryzhov, I.Y.; Verkhoturov, A.A.; Spears, D.A.; Melkiy, V.A.; Zarubina, N.V.; Blokhin, M.G. Geochemistry and rare-metal potential of coals of the Sakhalin coal basin, Sakhalin Island, Russia. *Int. J. Coal Geol.* **2023**, *268*, 104197. [CrossRef]
32. Dai, S.; Zhou, Y.; Ren, D.; Wang, X.; Li, D.; Zhao, L. Geochemistry and mineralogy of the Late Permian coals from the Songzao Coalfield, Chongqing, southwestern China. *Sci. China Ser. D-Earth Sci.* **2007**, *50*, 678–688. [CrossRef]
33. Dai, S.; Ren, D.; Chou, C.-L.; Finkelman, R.B.; Seredin, V.V.; Zhou, Y. Geochemistry of trace elements in Chinese coals: A review of abundances, genetic types, impacts on human health, and industrial utilization. *Int. J. Coal Geol.* **2012**, *94*, 3–21. [CrossRef]
34. Dai, S.; Zou, J.; Jiang, Y.; Ward, C.R.; Wang, X.; Li, T.; Xue, W.; Liu, S.; Tian, H.; Sun, X.; et al. Mineralogical and geochemical compositions of the Pennsylvanian coal in the Adaohai Mine, Daqingshan Coalfield, Inner Mongolia, China: Modes of occurrence and origin of diaspore, gorceixite, and ammonian illite. *Int. J. Coal Geol.* **2012**, *94*, 250–270. [CrossRef]
35. Sun, B.; Zeng, F.; Moore, T.A.; Rodrigues, S.; Liu, C.; Wang, G. Geochemistry of two high-lithium content coal seams, Shanxi Province, China. *Int. J. Coal Geol.* **2022**, *260*, 104059. [CrossRef]
36. Wang, N.; Dai, S.; Nechaev, V.P.; French, D.; Graham, I.T.; Song, X.; Chekryzhov, I.Y.; Tarasenko, I.A.; Budnitskiy, S.Y. Detrital U-Pb zircon geochronology, zircon Lu-Hf and Sr-Nd isotopic signatures of the Lopingian volcanic-ash-derived Nb-Zr-REY-Ga mineralized horizons from eastern Yunnan, SW China. *Lithos* **2024**, *468–469*, 107494. [CrossRef]
37. Wang, Q.; Dai, S.; Nechaev, V.P.; French, D.; Graham, I.; Zhao, L.; Zhang, S.; Liang, Y.; Hower, J.C. Transformation of organic to inorganic nitrogen in NH_4^+-illite-bearing and Ga-Al-REE-rich bituminous coals: Evidence from nitrogen isotopes and functionalities. *Chem. Geol.* **2024**, *660*, 122169. [CrossRef]
38. Zhang, S.; Yuan, T.; Sun, B.; Li, L.; Ma, X.; Shi, S.; Liu, Q. Formation of boehmite through desilication of volcanic-ash-altered kaolinite and its retention for gallium: Contribution to enrichment of aluminum and gallium in coal. *Int. J. Coal Geol.* **2024**, *281*, 104404. [CrossRef]
39. Zhao, L.; Dai, S.; Nechaev, V.P.; Nechaeva, E.V.; Graham, I.T.; French, D.; Sun, J. Enrichment of critical elements (Nb-Ta-Zr-Hf-REE) within coal and host rocks from the Datanhao mine, Daqingshan Coalfield, northern China. *Ore Geol. Rev.* **2019**, *111*, 102951. [CrossRef]
40. Zhao, L.; Dai, S.; Nechaev, V.P.; Nechaeva, E.V.; Graham, I.T.; French, D. Enrichment origin of critical elements (Li and rare earth elements) and a Mo-U-Se-Re assemblage in Pennsylvanian anthracite from the Jincheng Coalfield, southeastern Qinshui Basin, northern China. *Ore Geol. Rev.* **2019**, *115*, 103184. [CrossRef]
41. Finkelman, R.B.; Palmer, C.A.; Wang, P. Quantification of the modes of occurrence of 42 elements in coal. *Int. J. Coal Geol.* **2018**, *185*, 138–160.
42. Finkelman, R.B.; Wolfe, A.; Hendryx, M.S. The future environmental and health impacts of coal. *Energy Geosci.* **2021**, *2*, 99–112. [CrossRef]
43. Bi, X.Y.; Li, Z.G.; Wang, S.X.; Zhang, L.; Xu, R.; Liu, J.L.; Yang, H.; Guo, M.Z. Lead isotopic compositions of selected coals, Pb/Zn ores and fuels in China and the application for source tracing. *Environ. Sci. Technol.* **2017**, *51*, 13502–13508. [CrossRef] [PubMed]
44. Dai, S.; Ren, D.; Chou, C.-L.; Li, S.; Jiang, Y. Mineralogy and geochemistry of the no. 6 coal (Pennsylvanian) in the Junger Coalfield, Ordos Basin, China. *Int. J. Coal Geol.* **2006**, *66*, 253–270. [CrossRef]
45. Dai, S.; Hower, J.; Ward, C.R.; Guo, W.; Song, H.; O'Keefe, J.M.K.; Xie, P.; Hood, M.M.; Yan, X. Elements and phosphorus minerals in the middle Jurassic inertinite-rich coals of the Muli Coalfield on the Tibetan Plateau. *Int. J. Coal Geol.* **2015**, *144*, 23–47. [CrossRef]
46. Hower, J.C.; Williams, D.A.; Eble, C.F.; Sakulpitakphon, T.; Moecher, D.P. Brecciated and mineralized coals in Union County, Western Kentucky coal field. *Int. J. Coal Geol.* **2001**, *47*, 223–234. [CrossRef]
47. Swaine, D.J. The organic association of elements in coals. *Org. Geochem.* **1992**, *18*, 259–261. [CrossRef]
48. Zhou, G.; Jiang, Y.; Liu, M. Sapropelic coal petrologic, quality and trace element characteristics in Datun mining area, Xuzhou. *Coal Geol. China* **2011**, *23*, 7–9. (In Chinese)

49. Dai, Y.; Zhu, J.; Tan, D.; Ren, K.; Tao, F.; Wang, J. Preliminary investigation on concentration and isotopic composition of lead in coal from Guizhou Province, China. *Earth Env.* **2017**, *45*, 290–297.
50. Dai, S.; Tian, L.; Chou, C.-L.; Zhou, Y.; Zhang, M.; Zhao, L.; Wang, J.; Yang, Z.; Cao, H.; Ren, D. Mineralogical and compositional characteristics of Late Permian coals from an area of high lung cancer rate in Xuan Wei, Yunnan, China: Occurrence and origin of quartz and chamosite. *Int. J. Coal Geol.* **2008**, *76*, 318–327. [CrossRef]
51. Díaz-Somoano, M.; Kylander, M.E.; López-Antón, M.A.; Suárez-Ruiz, I.; Martínez-Tarazona, M.R.; Ferrat, M.; Kober, B.; Weiss, D.J. Stable lead isotope compositions in selected coals from around the world and implications for present day aerosol source tracing. *Environ. Sci. Technol.* **2009**, *43*, 1078–1085. [CrossRef]
52. Díaz-Somoano, M.; Suárez-Ruiz, I.; Alonso, J.I.G.; Encinar, J.R.; López-Antón, M.A.; Martínez-Tarazona, M.R. Lead isotope ratios in Spanish coals of different characteristics and origin. *Int. J. Coal Geol.* **2007**, *71*, 28–36. [CrossRef]
53. Mihaljevič, M.; Ettler, V.; Strnad, L.; Šebek, O.; Vonásek, F.; Drahota, P.; Rohovec, J. Isotopic composition of lead in Czech coals. *Int. J. Coal Geol.* **2009**, *78*, 38–46. [CrossRef]
54. Ward, C.R. Analysis and significance of mineral matter in coal seams. *Int. J. Coal Geol.* **2002**, *50*, 135–168. [CrossRef]
55. Ward, C.R. Analysis, origin and significance of mineral matter in coal: An updated review. *Int. J. Coal Geol.* **2016**, *165*, 1–27. [CrossRef]
56. Chitlango, F.Z.; Wagner, N.J.; Moroeng, O.M. Characterization and pre-concentration of rare earth elements in density fractionated samples from the Waterberg Coalfield, South Africa. *Int. J. Coal Geol.* **2023**, *275*, 104299. [CrossRef]
57. Willard, D.A.; Ruppert, L.F. Broadening the perspectives of sedimentary organic matter analysis to understand Earth system response to change. *Int. J. Coal Geol.* **2023**, *274*, 104281. [CrossRef]
58. Finkelman, R.B.; Dai, S.; French, D. The importance of minerals in coal as the hosts of chemical elements: A review. *Int. J. Coal Geol.* **2019**, *212*, 103251. [CrossRef]
59. Jiu, B.; Jin, Z.; Wang, Z. Multiscale in-situ elemental characterization of critical elements in low rank coal, implications for modes of occurrence. *Fuel* **2023**, *349*, 128632. [CrossRef]
60. Qin, G.; Cao, D.; Wei, Y.; Wang, A.; Liu, J. Geochemical characteristics of the Permian coals in the Junger-Hebaopian mining district, northeastern Ordos Basin, China: Key role of paleopeat-forming environments in Ga-Li-REY enrichment. *J. Geochem. Explor.* **2020**, *213*, 106494. [CrossRef]
61. Hayashi, K.I.; Fujisawa, H.; Holland, H.D.; Ohmoto, H. Geochemistry of ~1.9 Ga sedimentary rocks from northeastern Labrador, Canada. *Geochim. Cosmochim. Acta* **1997**, *61*, 4115–4137.
62. Dai, S.; Wang, X.; Zhou, Y.; Hower, J.C.; Li, D.; Chen, W.; Zhu, X.; Zou, J. Chemical and mineralogical compositions of silicic, mafic, and alkali tonsteins in the late Permian coals from the Songzao Coalfield, Chongqing, Southwest China. *Chem. Geol.* **2011**, *282*, 29–44. [CrossRef]
63. Dai, S.; Li, T.; Jiang, Y.; Ward, C.R.; Hower, J.C.; Sun, J.; Liu, J.; Song, H.; Wei, J.; Li, Q.; et al. Mineralogical and geochemical compositions of the Pennsylvanian coal in the Hailiushu Mine, Daqingshan Coalfield, Inner Mongolia, China: Implications of sediment-source region and acid hydrothermal solutions. *Int. J. Coal Geol.* **2015**, *137*, 92–110. [CrossRef]
64. Dai, S.; Yang, J.; Ward, C.R.; Hower, J.C.; Liu, H.; Garrison, T.M.; French, D.; O'Keefe, J.M. Geochemical and mineralogical evidence for a coal-hosted uranium deposit in the Yili Basin, Xinjiang, northwestern China. *Ore Geol. Rev.* **2015**, *70*, 1–30. [CrossRef]
65. Zhou, M.; Dai, S.; Wang, X.; Zhao, L.; Nechaev, V.P.; French, D.; Graham, I.T.; Zheng, J.; Wang, Y.; Dong, M. Critical element (Nb-Ta-Zr-Hf-REE-Ga-Th-U) mineralization in Late Triassic coals from the Gaosheng Mine, Sichuan Basin, southwestern China: Coupled effects of products of sediment-source-region erosion and acidic water infiltration. *Int. J. Coal Geol.* **2022**, *262*, 104101. [CrossRef]
66. Dai, S.; Seredin, V.V.; Ward, C.R.; Hower, J.C.; Xing, Y.; Zhang, W.; Song, W.; Wang, P. Enrichment of U–Se–Mo–Re–V in coals preserved within marine carbonate successions: Geochemical and mineralogical data from the Late Permian Guiding Coalfield, Guizhou, China. *Miner. Depos.* **2015**, *50*, 159–186. [CrossRef]
67. Ketris, M.Á.; Yudovich, Y.E. Estimations of Clarkes for Carbonaceous biolithes: World averages for trace element contents in black shales and coals. *Int. J. Coal Geol.* **2009**, *78*, 135–148. [CrossRef]
68. Shen, M.; Dai, S.; French, D.; Graham, I.T.; Spiro, B.F.; Wang, N.; Tian, X. Geochemical and mineralogical evidence for the formation of siderite in late Permian coal-bearing strata from western Guizhou, SW China. *Chem. Geol.* **2023**, *637*, 121675. [CrossRef]
69. Shen, M.; Dai, S.; Nechaev, V.P.; French, D.; Graham, I.T.; Liu, S.; Chekryzhov, I.Y.; Tarasenko, I.A.; Zhang, S. Provenance changes for mineral matter in the latest Permian coals from western Guizhou, southwestern China, relative to tectonic and volcanic activity in the Emeishan Large Igneous Province and Paleo-Tethys region. *Gondwana Res.* **2023**, *113*, 71–88. [CrossRef]
70. Chen, H.; He, S.; Zhang, A.; Sun, J.; Yan, Z.; Liu, J.; Zhang, L.; Qian, Y. Petrogenesis and tectonic setting of Middle Silurian A-type granite in Kaerqueka area, East Kunlun. *Geol. Bull. China* **2021**, *40*, 1380–1393.
71. Seredin, V.V.; Dai, S. Coal deposits as potential alternative sources for lanthanides and yttrium. *Int. J. Coal Geol.* **2012**, *94*, 67–93. [CrossRef]
72. Qin, S.J.; Gao, K.; Wang, J.X.; Li, Y.H.; Lu, Q.F. Geochemistry of the associated elements in the Late Permian Coal from the Huoshaopu and Jinjia Mines, Southwestern Guizhou. *China Coal Soc.* **2016**, *41*, 1507–1516.

73. Liu, J.; Nechaev, V.P.; Dai, S.; Song, H.; Nechaeva, E.V.; Jiang, Y.; Graham, I.T.; French, D.; Yang, P.; Hower, J.C. Evidence for multiple sources for inorganic components in the Tucheng coal deposit, western Guizhou, China and the lack of critical-elements. *Int. J. Coal Geol.* **2020**, *223*, 103468. [CrossRef]
74. Nechaev, V.P.; Dai, S.; Chekryzhov, I.Y.; Tarasenko, I.A.; Zin'kov, A.V.; Moore, T.A. Origin of the tuff parting and associated enrichments of Zr, REY, redox-sensitive and other elements in the Early Miocene coal of the Siniy Utyes Basin, southwestern Primorye, Russia. *Int. J. Coal Geol.* **2022**, *250*, 103913. [CrossRef]
75. Shen, M.; Dai, S.; Graham, I.T.; Nechaev, V.P.; French, D.; Zhao, F.; Shao, L.; Liu, S.; Zuo, J.; Zhao, J.; et al. Mineralogical and geochemical characteristics of altered volcanic ashes (tonsteins and K-bentonites) from the latest Permian coal-bearing strata of western Guizhou Province, southwestern China. *Int. J. Coal Geol.* **2021**, *237*, 103707. [CrossRef]
76. Wang, N.; Dai, S.; Wang, X.; Nechaev, V.P.; French, D.; Graham, I.T.; Zhao, L.; Song, X. New insights into the origin of Middle to Late Permian volcaniclastics (Nb-Zr-REY-Ga-rich horizons) from eastern Yunnan, SW China. *Lithos* **2022**, *420–421*, 106702. [CrossRef]
77. Taylor, S.R.; McLennan, S.M. *The Continental Crust: Its Composition and Evolution*; U.S. Department of Energy: Oak Ridge, TN, USA, 1985.
78. Dai, S.; Graham, I.T.; Ward, C.R. A review of anomalous rare earth elements and yttrium in coal. *Int. J. Coal Geol.* **2016**, *159*, 82–95. [CrossRef]
79. Dai, S.; Seredin, V.V.; Ward, C.R.; Jiang, J.; Hower, J.C.; Song, X.; Jiang, Y.; Wang, X.; Gornostaeva, T.; Li, X.; et al. Composition and modes of occurrence of minerals and elements in coal combustion products derived from high-Ge coals. *Int. J. Coal Geol.* **2014**, *121*, 79–97. [CrossRef]
80. Patra, K.C.; Rautray, T.R.; Tripathy, B.B.; Nayak, P. Elemental analysis of coal and coal ASH by PIXE technique. *Appl. Radiat. Isot.* **2012**, *70*, 612–616. [CrossRef] [PubMed]
81. Qiao, J.; Du, F.; Wang, S.; Tan, F.; Zhang, Y. Enrichment and Occurrence of Mn in 5^{-2} Coal from Qinglongsi Coal Mine, Northern Ordos Basin, China. *ACS Omega* **2020**, *5*, 20202–20214. [CrossRef]
82. Finkelman, R.B. Trace elements in coal: Environmental and health significance. *Biol. Trace Elem. Res.* **1999**, *67*, 197–204. [CrossRef]
83. Liu, J.; Ward, C.R.; Graham, I.T.; French, D.; Dai, S.; Song, X. Modes of occurrence of non-mineral inorganic elements in lignites from the Mile Basin, Yunnan Province, China. *Fuel* **2018**, *222*, 146–155. [CrossRef]
84. Dai, S.; Wang, P.; Ward, C.R.; Tang, Y.; Song, X.; Jiang, J.; Hower, J.C.; Li, T.; Seredin, V.V.; Wagner, N.J.; et al. Elemental and mineralogical anomalies in the coal-hosted Ge ore deposit of Lincang, Yunnan, southwestern China: Key role of N_2-CO_2-mixed hydrothermal solutions. *Int. J. Coal Geol.* **2015**, *152*, 19–46. [CrossRef]
85. Shao, P.; Hou, H.; Wang, W.; Qin, K.; Wang, W. Distribution and enrichment of Al-Li-Ga-REEs in the High-Alumina coal of the Datong Coalfield, Shanxi Province, China. *Ore Geol. Rev.* **2022**, *140*, 104597. [CrossRef]
86. Sun, B.; Guo, Z.; Liu, C.; Kong, Y.; French, D.; Zhu, Z. Lithium isotopic composition of two high-lithium coals and their fractions with different lithium occurrence modes, Shanxi Province, China. *Int. J. Coal Geol.* **2023**, *277*, 104338. [CrossRef]
87. Xu, F.; Qin, S.; Li, S.; Wen, H.; Lv, D.; Wang, Q.; Kang, S. The migration and mineral host changes of lithium during coal combustion: Experimental and thermodynamic calculation study. *Int. J. Coal Geol.* **2023**, *275*, 104298. [CrossRef]
88. Finkelman, R.B. Modes of occurrence of environmentally-sensitive trace elements in coal. In *Environmental Aspects of Trace Elements in Coal*; Springer: Dordrecht, The Netherlands, 1995; pp. 24–50.
89. Çelebi, E.E.; Ribeiro, J. Prediction of acid production potential of self-combusted coal mining wastes from Douro Coalfield (Portugal) with integration of mineralogical and chemical data. *Int. J. Coal Geol.* **2023**, *265*, 104152. [CrossRef]
90. Matýsek, D.; Jirásek, J. Mineralogy of the coal waste dumps from the Czech part of the Upper Silesian Basin: Emphasized role of halides for element mobility. *Int. J. Coal Geol.* **2022**, *264*, 104138. [CrossRef]
91. Yang, P.; Dai, S.; Nechaev, V.P.; Song, X.; Chekryzhov, I.Y.; Tarasenko, I.A.; Tian, X.; Yao, M.; Kang, S.; Zheng, J. Modes of occurrence of critical metals (Nb-Ta-Zr-Hf-REY-Ga) in altered volcanic ashes in the Xuanwei Formation, eastern Yunnan Province, SW China: A quantitative evaluation based on sequential chemical extraction. *Ore Geol. Rev.* **2023**, *160*, 105617. [CrossRef]
92. Arnold, B.J. A review of element partitioning in coal preparation. *Int. J. Coal Geol.* **2023**, *274*, 104296. [CrossRef]
93. Xu, N.; Xu, C.; Finkelman, R.B.; Engle, M.A.; Li, Q.; Peng, M.; He, L.; Huang, B.; Yang, Y. Coal elemental (compositional) data analysis with hierarchical clustering algorithms. *Int. J. Coal Geol.* **2022**, *249*, 103892. [CrossRef]
94. Zhu, B.Q. *Theory and Application of Isotope System in Earth Science: Also on the Evolution of the Crust and Mantle of the Chinese Mainland*; Science Press: Beijing, China, 1998. (In Chinese)
95. Zartman, R.E.; Doe, B.R. Plumbotectonics—The model. *Tectonophysics* **1981**, *75*, 135–162. [CrossRef]

Disclaimer/Publisher's Note: The statements, opinions and data contained in all publications are solely those of the individual author(s) and contributor(s) and not of MDPI and/or the editor(s). MDPI and/or the editor(s) disclaim responsibility for any injury to people or property resulting from any ideas, methods, instructions or products referred to in the content.